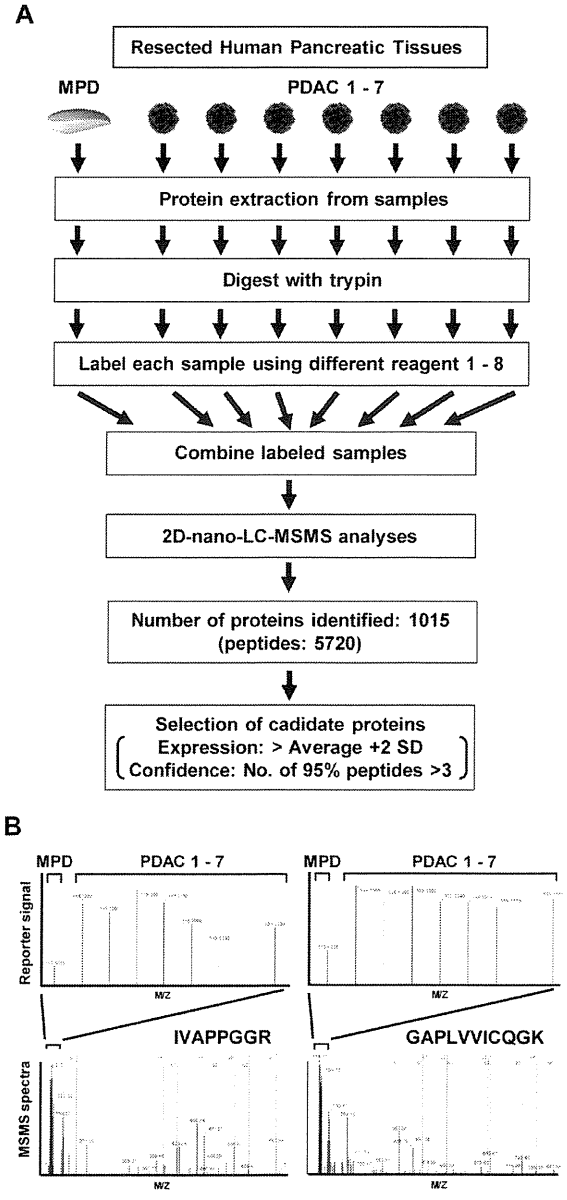

Fig. 1 Kawahara et al.

Figure 1. Identification of differentially expressed DPYSL3 in pancreatic ductal adenocarcinoma. (A) Workflow for identification of proteins differentially expressed between pancreatic ductal adenocarcinoma and main pancreatic ductal tissues. Protein Pilot is a program designed for maximizing information obtained from iTRAQ tagging and MS/MS quantification. (B) Spectra obtained from quantification (upper panel) and MS/MS sequencing (lower panel) of representative peptides from DPYSL3 using the Protein Pilot program. MPD, main pancreatic duct; PDAC, pancreatic ductal adenocarcinoma.

doi: 10.1371/journal.pone.0079654.g001

examine this, we employed flow cytometry (FCM) following annexin V-FITC staining. Adhered cells were collected with or without floating cells, then subjected to FCM assays. As shown in Figure 3F, more frequent induction of apoptosis was observed in adhered cells with floating cells treated with siDPYSL3 as compared with the siControl-treated cells. We also analyzed the number of floating cells treated with siControl and siDPYSL3, and found that a much larger number was detached from the bottoms of the dishes after treatment with siDPYSL3 (Figure 3G, left panel). Furthermore, we analyzed the frequency of annexin V-FITC stained cells among floating cells treated with siDPYSL3. As shown in Figure 3G (right panel), 60-70% of the siDPYSL3-treated floating cells were positive for annexin V-FITC staining. These results showed that the floating cells were originally viable and then died from apoptosis.

DPYSL3 regulates cell adhesion, motility, and invasion in pancreatic cancer cells

Since a dysfunction of cellular adhesion was observed in pancreatic cancer cells treated with siDPYSL3, we further examined the role of DPYSL3 in cell adhesion. Exogenous expression of DPYSL3 in PANC-1 cells, which show no endogenous expression of DPYSL3, increased the number of cells adhered to fibronectin (Figure 4A). This finding prompted us to investigate the characteristics of focal adhesion, which consists of protein complexes including Integrin, focal adhesion kinase (FAK) and adaptor proteins such as Vinculin and Talin1 (TLN1). As shown in Figure 4B, exogenous expression of DPYSL3 in PANC-1 cells promoted formation of larger areas of focal adhesion as compared with the vector control, supporting the notion that DPYSL3 is a regulatory molecule of cellular adhesion. Since focal adhesion is known to regulate cell migration, we next investigated the role of DPYSL3 in pancreatic cancer cell migration and found acquisition of the enhanced motile phenotype in DPYSL3-introduced PANC-1 cells *in vitro*, as shown by a motility assay (Figure 4C) as well as a matrigel invasion assay (Figure 4D). We further evaluated the effects of DPYSL3 on metastasis using a DPYSL3-positive pancreatic cancer cell line, CFPAC-1. CFPAC-1 cells were treated with siDPYSL3 for 24 hours, then injected into the tail vein of mice, which showed significantly reduced experimental lung metastasis at 48 hours after injection (Figure 4E and 4F). We also evaluated the effects of DPYSL3 on metastasis using a DPYSL3-positive highly metastatic lung cancer cell line, NCI-H460-LNM35, which we previously generated through *in vivo* selection [8]. NCI-H460-LMN35 cells were treated with siDPYSL3 for 24 hours, then subjected to a matrigel invasion assay as well as an experimental metastasis assay, which showed significantly reduced the metastatic ability (Figure S5).

DPYSL3 interacts with Ezrin and regulates stability of adhesion complex

Our observations revealed that DPYSL3 regulated the adhesion and migration abilities of pancreatic cancer cells *in vitro* as well as metastasis *in vivo*. In order to gain insight into the molecular function of DPYSL3, we employed *in vitro* protein-protein binding assays, followed by comprehensive

Table 1. Result from protein expression profiling of patients with pancreatic cancer in the discovery cohort.

Accession #	Name	Peptides(95%)	PDAC119/3MPD	PDAC120/3MPD	PDAC122/3MPD	PDAC123/3MPD	PDAC136/3MPD	PDAC138/3MPD	PDAC139/3MPD
IPI00872788	DPYSL3	4	**5.8236**	**4.0091**	**4.8231**	**4.213**	**4.875**	**3.6861**	**3.6631**
IPI00515061	HIST1H2BJ	9	**6.3658**	**5.1424**	**9.2206**	**5.9593**	**8.2686**	**6.5239**	**6.3418**
IPI00219757	GSTP1	5	**5.2444**	**6.9614**	**5.863**	**3.408**	**3.6595**	**7.7206**	**7.011**
IPI00012011	CFL1	4	4.1628	3.1135	3.4594	**4.0643**	**3.3542**	**4.618**	**4.9594**
IPI00552873	HIST1H2AL	5	**4.8203**	**5.241**	3.267	2.2544	3.1102	**5.5493**	**5.2892**
IPI00018146	14-3-3 protein theta	5	1.5423	1.3871	2.2262	**5.2277**	**5.2819**	**3.7495**	**5.7482**
IPI00023006	ACTC1	31	4.2576	**4.3199**	2.4028	**3.1457**	2.7104	**12.315**	**7.8559**
IPI00021263	14-3-3 protein zeta/delta	7	2.642	2.6519	3.3913	**3.1726**	2.8626	**4.0071**	**3.8538**
IPI00647915	TAGLN2	7	4.0373	3.2737	3.0549	2.311	**3.6478**	**4.2864**	**4.0487**
IPI00217465	HIST1H1C	6	2.5444	2.149	**4.4859**	**3.952**	3.019	1.5961	1.829
IPI00645452	TUBB	9	3.3303	**4.1586**	2.3707	2.5416	**4.2104**	3.2809	2.3754
IPI00927101	RPSAP15	3	3.0867	1.7409	3.2011	**3.4315**	**3.9153**	3.1611	2.9445
IPI00553177	SERPINA1	6	2.8568	3.9234	3.3977	**4.8721**	**3.5474**	3.5953	3.3685
IPI00479186	PKM2	23	2.4052	1.9882	1.7363	2.0183	2.3442	**3.9284**	**3.8285**
IPI00027463	S100A6	3	2.0807	3.1992	2.2405	1.0219	1.5851	**4.8025**	**3.9427**
IPI00171611	HIST2H3A	4	1.7747	1.5673	1.2974	1.9209	2.9463	**3.8263**	**3.9559**
IPI00910262	POSTN	8	2.2295	2.0132	1.7284	1.0481	2.9901	**3.8061**	**4.316**
IPI00306959	KRT7	12	1.5053	2.093	2.2755	0.7767	0.9113	**5.0483**	**4.3531**
IPI00013808	ACTN4	18	1.6111	1.828	1.484	1.2117	1.592	**8.6536**	**5.8044**

Value shows relative expression ratio of each protein in PDAC patients compared to MPD. Value written in bold is greater than average + 2SD in protein expression profile of each PDAC specimen.

doi: 10.1371/journal.pone.0079654.t001

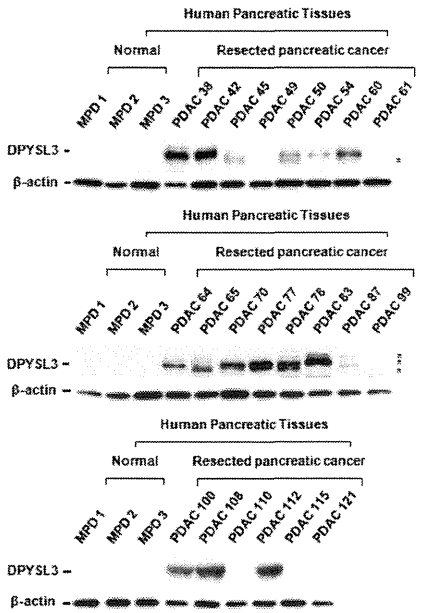

Fig. 2 Kawahara et al.

Figure 2. Verification of proteomic data by western blot analyses using independent PDAC tissue specimens. DPYSL3 protein expression in human PDAC tissues not used for the discovery phase with iTRAQ tagging and MS/MS quantification was analyzed by western blotting. MPD, main pancreatic duct; PDAC, pancreatic ductal adenocarcinoma. *Alternative transcriptional variant of DPYSL3.

doi: 10.1371/journal.pone.0079654.g002

protein profiling using mass spectrometry (Figure S6A). A total of 17 proteins in the lysate of CFPAC-1 cells were found to be candidate molecules that interact with DPYSL3 (Table S4). To evaluate the significance of their interactions with DPYSL3, we further employed MRM analyses for precise quantification of the concentrations of the proteins of interest in the eluate from the GST-tagged DPYSL3-affinity column as well as from the purified GST-affinity column (Table S4). Consequently, Ezrin (EZR), a cytoplasmic peripheral membrane protein that is known to play a key role in cell surface structure adhesion and migration via activation of FAK and c-Src in the adhesion complex [17–19], was found at higher level in the eluate from the DPYSL3-affinity column, to which the CFPAC-1 cell lysate was applied, than in the eluate from the purified GST-affinity column (Figure 5A and Figure S6B). While a neuroblast differentiation-associated protein (AHNK) (Figure 5B), as well as Vimentin and Lamin-A were also found at higher level in the eluate from the DPYSL3-affinity column, rest of the candidates were not detected in the eluate from the DPYSL3-affinity column (Figure S6C). Since candidate DPYSL3 interacting

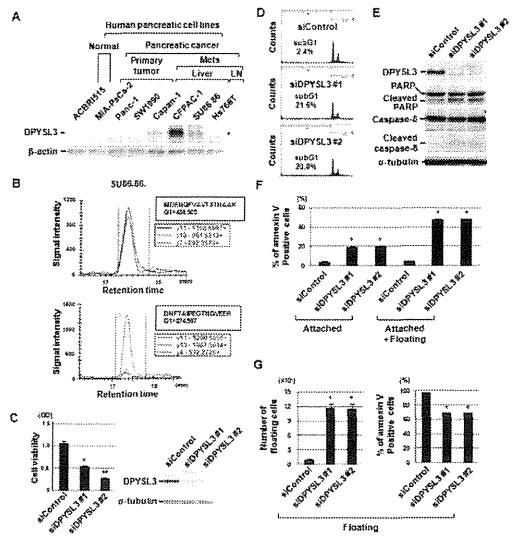

Fig. 3 Kawahara et al.

Figure 3. Involvement of DPYSL3 in pancreatic cancer cell survival. (A) DPYSL3 protein expression in human pancreatic cancer cell lines was analyzed by western blotting. β-actin was used as a loading control. (B) MRM analyses using two established transitions revealed that DPYSL3 existed in a SU86.86 cell line. (C) siDPYSL3 treatment induced significant growth inhibition of a CFPAC-1 pancreatic cancer cell line that highly expressed DPYSL3 (left panel). Western blotting showed that DPYSL3 expression was efficiently knocked down by treatment with siDPYSL3. Two different siDPYSL3 proteins (#1 and #2) were used to clarify the specificity of the effect of siRNA-mediated DPYSL3 knockdown. Data are shown as the mean ± SD (n=3). *p <0.002 versus siControl, **p <0.001 versus siControl (Student's t test). (D) Flow-cytometric analysis showed an increase in the sub-G1 population of CFPAC-1 cells after introduction of siDPYSL3. (E) Western blot analysis showed increased expression of cleaved-PARP and -caspase-8 in siDPYSL3-treated CFPAC-1 cells. (F) Flow-cytometric analysis combined with immunofluorescent staining using annexin V-FITC showed an increase in apoptotic cell death of CFPAC-1 cells after introduction of siDPYSL3. Data are shown as the mean ± SD (n=3). *p <0.001 versus siControl (Student's t test). (G) siDPYSL3 treatment induced dysfunctions in cellular adhesion and apoptotic cell death. Floating cells were collected from condition media and the number of cells were counted (left panel). Floating cells were also subjected to flow-cytometric analysis combined with immunofluorescent staining using annexin V-FITC showed a significant increase in apoptotic cell death among detached CFPAC-1 cells after introduction of siDPYSL3. Data are shown as the mean ± SD (n=3). *p <0.001 versus siControl (Student's t test).

doi: 10.1371/journal.pone.0079654.g003

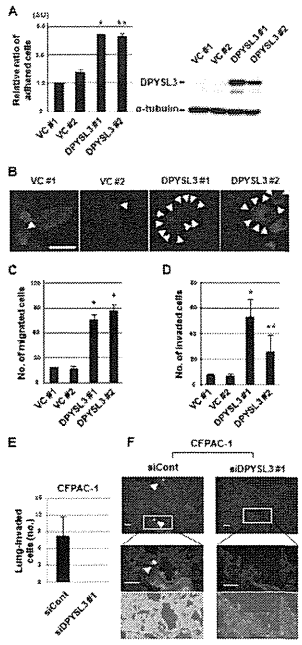

Fig. 4 Kawahara et al.

Figure 4. DPYSL3 regulates cell adhesion, motility, and invasion abilities of pancreatic cancer cells. (A) Overexpression of DPYSL3 in PANC-1 cells, which initially showed no expression of DPYSL3, increased the number of cells to adhered fibronectin. Data are shown as the mean ± SD (n=3). DPYSL3 #1 and #2, stable transfectants of DPYSL3 in PANC-1cells; VC #1 and #2, stable transfectants of empty vector in PANC-1cells; *p <0.001 vs. average of VC (Student's t test). (B) Immunofluorescence staining of vinculin in DPYSL3-expressing PANC-1 cells. Scale bar = 10 μm. Exogenous expression of DPYSL3 in Panc-1 cells promoted formation of larger focal adhesions (arrow heads) as compared with the vector control, supporting the notion that DPYSL3 is the regulatory molecule of cellular adhesion. (C and D) Acquisition of a motile phenotype in DPYSL3-expressing PANC-1 cells was clearly demonstrated by results of a motility assay (C) as well as those of a matrigel invasion assay (D). Data are shown as the mean ± SD (n=5). *p <0.001 vs. average of VC, **p <0.016 vs. average of VC (Student's t test). (E) Experimental metastasis assay of CFPAC-1 cells knocked down for DPYSL3 with siDPYSL3 #1 (five mice per treatment). Five thin slices were obtained from each mouse lung specimen and images (x20) of each slice were obtained. The number of fluorescent-positive cancer cells was counted and determined for each mouse, then the average value for each treatment was calculated. Bars show the mean ± SD. *p <0.001 vs. average of siControl (Student's t test). (F) Representative fluorescence images of perfusion-resistant cells. Cells were stained with calcein. Magnified fluorescence images (middle panel) and phase contrast micrographs (lower panel) are shown. Scale bars indicate 50 μm.

doi: 10.1371/journal.pone.0079654.g004

proteins, identified from proteomic analyses using the GST-tagged DPYSL3 affinity column, may contain non-specific GST tag interacting proteins, we further examined the interaction between DPYSL3 and EZR in PANC-1 cells stably transfected with myc-tagged DPYSL3 using immunoprecipitation-western blot (IP-WB) analysis. As shown in Figure 5C, we confirmed a clear interaction between DPYSL3 and EZR using the anti-myc-tag antibody targeting myc-tagged DPYSL3, which showed that this interaction was specific. Since EZR is crucially involved in formation of an adhesion complex thought to play an important role in development of the metastatic phenotype, we investigated whether DPYSL3 participates in that adhesion complex. We observed that constituents of the adhesion complex, such as FAK, TLN1 and c-Src, were co-immunoprecipitated with DPYSL3 (Figure 5C). Reciprocally, IP-WB analysis using the anti-EZR antibody for IP showed that exogenous expression of DPYSL3 in PANC-1 cells stabilized the interaction between EZR and constituents of the adhesion complex (Figure 5D). Therefore, our results strongly suggest that DPYSL3 is included in the adhesion complex and stabilizes its formation.

Lastly, we investigated the effects of DPYSL3 expression on tyrosine phosphorylation of EZR (Y145), which is known to be involved in the regulation of cell adhesion, spreading, and proliferation [19]. We consequently observed a reduction of phosphorylation of EZR (Y145) in response to DPYSL3 knockdown in CFPAC-1 cells (Figure 5E, left panel). Conversely, exogenous overexpression of DPYSL3 increased the level of phosphorylated-EZR (Y145) in PANC-1 cells with low DPYSL3 expression (Figure 5E, middle panel). c-Src is a kinase known to be responsible for phosphorylation of the Y145 site on EZR, and phosphorylated EZR (Y145) in turn plays a role in maintenance of activated phosphorylation of c-Src at the Y416 residue [19]. We therefore analyzed the level of phosphorylation of c-Src (Y416) in siDPYSL3-treated CFPAC-1 cells as well as in stable transfectants of PANC-1 cells expressing exogenous DPYSL3. As shown in Figure 5E (left panel), DPYSL3 knockdown resulted in reduced phosphorylation of c-Src (Y416) in CFPAC-1 cells, while exogenous expression of DPYSL3 upregulated the level of phosphorylation of c-Src (Y416) in PANC-1 cells (Figure 5D, middle panel). For further confirmation, we treated PANC-1 cells stably expressing exogenous DPYSL3 with siDPYSL3 and observed that induction of phosphorylated-c-Src (Y416) was cancelled by knockdown of DPYSL3 (Figure 5E, right panel). Taken together, the present findings indicate that DPYSL3 highly expressed in PDAC interacts with EZR and promotes phosphorylations of EZR and c-Src via interaction with EZR as well as with constituents of the adhesion complex. Furthermore, this stabilization of the adhesion complex confers increased adhesion, motility, and invasion abilities to pancreatic cancer cells, which characteristically exhibit highly metastatic phenotypes.

Discussion

A major challenge in the management of PDAC patients is the nearly inevitable occurrence of tumor metastasis, even in

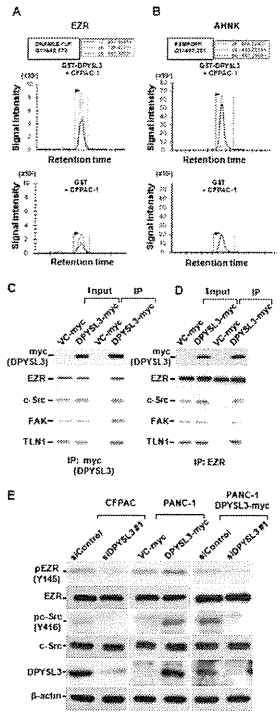

Fig. 5 Kawahara et al.

Figure 5. DPYSL3 interacts with EZR and regulates stability of adhesion complex. (A and B) MRM analyses revealed that EZR and AHNK were deteted at higher level in the eluate from the DPYSL3-affinity column to which the CFPAC-1 cell lysate was applied. Eluate samples from the affinity columns were subjected to MRM analysis using an established transition protocol for detection of EZR and AHNK. A clear signal of EZR was observed in that from the DPYSL3-GST-affinity column (A, upper panel). A clear signal of AHNK was observed in that from the DPYSL3-GST-affinity column (B, upper panel). The X-axis shows retention time and y axis signal intensity of the detected products, which reflect the amounts of the peptides of interest. DPYSL3-GST (+), a lysate of Sf9 cells expressing GST-DPYSL3, was applied to glutathione beads; GST, a lysate of Sf9 cells together with purified GST protein, was applied to glutathione beads; CFPAC (+), a lysate of CFPAC-1 cells, was applied to the column. (C) IP-WB analyses using the anti-c-myc antibody for IP in stably DPYSL3-myc transfected PANC-1 cells revealed a clear interaction between DPYSL3 and EZR. FAK, TLN1, and c-Src, constituents of the adhesion complex, were also co-precipitated with DPYSL3. (D) IP-WB analysis using the anti-EZR antibody for IP showed that exogenous expression of DPYSL3 in Panc-1 cells stabilized the interactions between EZR and constituents of the adhesion complex. (E) Western blot analysis showed reduction of phosphorylation of EZR Y145 and c-Src Y416 in CFPAC-1 cells by DPYSL3 knockdown (left panel). Conversely, exogenous expression of DPYSL3 increased the levels of phosphorylated EZR Y145 and c-Src Y416 in PANC-1 cells (middle panel), while those effects were abrogated by simultaneous treatment with siDPYSL3 (right panel).

doi: 10.1371/journal.pone.0079654.g005

those who are considered to have undergone successful surgical resection. Tumor cells coordinate increased expression levels of metastasis-related genes, which promote cell adhesion, motility, and invasion [20]. The advent of mass spectrometry-based proteomic profiling, in which the expressions of hundreds of proteins can be simultaneously assessed, has greatly facilitated dissection of this process for better understanding of the pathophysiology of PDAC metastasis [11,21]. In the present study, we employed proteomic technologies combining mass spectrometry and peptide tagging to identify a set of proteins whose expression is associated with PDAC tumorigenesis, and identified DPYSL3 as a novel candidate protein. We further demonstrated that DPYSL3 regulates cancer cell migration and adhesion *in vitro* as well as metastasis *in vivo*, and plays an important role in formation of the adhesion complex. Although we clearly showed that functional significance of DPYSL3 in PDAC cells, it is possible that the expression of DPYSL3 occurs in tumor stroma cells or connective tissue with some functional relevance in tumor biology.

DPYSL3 is a member of the DPYSL family of cytosolic phosphoproteins, which mediates semaphorin/collapsin-induced growth cone collapse, and are also involved in axonal guidance and neuronal differentiation [22–24]. During the previous decade, 5 members of the DPYSL gene family (DPYSL1 to 5) encoding closely related 60-66 kDa proteins were isolated [25,26]. However, little is known about the functional significance of the DPYSL family in human malignancies. A previous study reported that DPYSL1 is an invasion suppressor and correlates with clinical outcomes in non-small-cell lung cancer, though the underlying molecular mechanisms of how DPYSL1 regulates the process of cancer metastasis have not been elucidated in detail [27,28]. Interestingly, we found that all three DPYSL3 positive PDAC cell lines were originated from liver metastasis (Capan-1, CFPAC-1 and SU86.86) in the western blotting assays, while Hs766T, originated from lymph node metastasis, does not express DPYSL3. On the other hand the expression of DPYSL3 was not detected in three cell lines originated from primary tumor (MIA PaCa-2, PANC-1 and SW 1990). These results are considered to support the notion that DPYSL3 plays a role in PDAC cell metastasis. In addition, DPYSL3 at 5q32 was recently found to correspond to 1 of 3 additional lung cancer susceptibility loci in a genome-wide association study [29], suggesting the possibility that DPYSL3 may be involved in development of lung cancer. It should also be noted that the molecular function of DPYSL3 in connection with cellular adhesion or stabilization of the adhesion complex has yet to be reported.

EZR is a cytoplasmic peripheral membrane protein that functions as a substrate of protein-tyrosine kinases, and also plays key roles in cellular adhesion and migration in the adhesion complex via activation of FAK and c-Src [17,18]. Phosphorylation is a crucial mechanism that regulates the function of EZR, with c-Src known to phosphorylate the Y145 site on EZR, while phosphorylated EZR (Y145) in turn maintains the activating phosphorylation of c-Src at Y416 residue, making cells active for adhesion, spreading, and

proliferation [19]. In the present study, we found that the levels of phosphorylation of EZR and c-Src are regulated by DPYSL3 in pancreatic cancer cells. In addition, the interaction between DPYSL3 and EZR was shown to play a role in stabilization of the adhesion complex that includes c-Src, FAK, and TLN1. Our findings suggest the possible existence of interplay among components of the focal adhesion complex, in which DPYSL3 is crucially involved, and regulates the adhesion and migration of pancreatic cancer cells. It is also of note that DPYSL3 contains a number of consensus phosphorylation sites that may serve as substrates for signaling molecules, such as Cdk, protein kinase C, and proline-directed kinases [23]. Therefore, it would be interesting to elucidate the detailed signaling pathway(s) leading to phosphorylation of DPYSL3 as well as the functional significance of that phosphorylation in the adhesion and migration processes of pancreatic cancer cells.

In the present study, we have shown that the expression of DPYSL3 protein is up-regulated in PDAC using combined proteomic approaches. Given that it has important roles in regulation of motile phenotype of pancreatic cancer cells, DPYSL3 may be an excellent candidate for anti-metastasis therapeutic strategies, which may ultimately lead to a reduction in the large number of deaths caused by this devastating disease.

Methods

Cell lines, pancreatic cancer tissues, protein extraction

MIA PaCa-2, PANC-1, SW 1990, CFPAC-1, SU86.86 and Hs766T (human pancreatic cancer cell lines) were purchased from ATCC and maintained in DMEM/10% fetal bovine serum (FBS). Capan-1 (human pancreatic cancer cells) was purchased from ATCC and cultured in IMDM/20% FBS, while ACBRI515 (human pancreatic epithelial cells) was purchased from Cell Systems (Kirkland, WA) and maintained in CS-C medium, which was changed to DMEM/10% FBS 48 hours before analysis. ATCC provided molecular authentication in support of their cell lines.

Tumor and normal main pancreatic ductal tissues (MPD) were collected from patients histologically diagnosed with primary pancreatic ductal adenocarcinoma (PDAC), and who underwent potentially curative resection at Nagoya University Hospital between February 2005 and October 2006. Staging was determined after pathologic evaluation of resected specimens according to the International System for Staging Pancreatic Cancer (Table S1 and S2). All tissues were quickly frozen in liquid nitrogen and stored at -80°C until analysis. All specimens were processed in the same manner. Similarly to the method we usually take for transcriptome analysis [3,5] , protein was isolated from frozen tissues of the tumor and normal MPD specimens, which were subjected to gross microdissection using 10-μm sections cut from frozen tissue samples on a cryostat at –20°C under the guidance of Giemsa staining to reduce contamination of the fibrotic areas and connective tissues using T-PER reagent (Pierce, Rockford, IL), according to the manufacturer's instructions. Quantities were checked using a Lowry assay (BioRad, Hercules, CA).

Ethics Statement

Approval from Nagoya University Hospital institutional review board and written informed consent from each patient were obtained. All animal experiments were approved by the Committee on the Ethics of Animal Experiments, Nagoya University Graduate School of Medicine, Japan.

Mass spectrometry analysis of iTRAQ discovery analyses

An overview of the workflow for the discovery phase is shown in Figure 1A. For iTRAQ labeling, 100 μg of protein extracted from the human resected tissues or cells were reduced, alkylated, and digested with trypsin according to the manufacturer's instructions (Applied Biosystems Inc., Foster city, CA). For discovery analyses, digested protein prepared from each sample was labeled with the iTRAQ reagent, then labeled samples were pooled and washed according to the manufacturer's instructions (Applied Biosystems Inc.).

Two-dimensional peptide fractionation was performed with a DiNa Direct Nano-flow LC system (KYA Technologies, Tokyo, Japan) using a strong cation exchange (SCX) column [HiQ sil SCX, 0.5-mm inside diameter (i.d.) x 35 mm], a reverse-phase (RP) trap column (HiQ Sil C18-3, 0.8-mm i.d. x 3 mm), and an RP analytical column (HiQ Sil C18-3 Gradient, 0.15-mm i.d. x 50 mm). Peptides trapped on the SCX column were eluted by injection of ammonium-formate (AF) buffer (pH 3.0, containing 2% acetonitrile) at various concentrations (10, 30, 50, 80, 100, 150, 200, 300, 500 mM). The eluate from each injection of AF buffer was directly subjected to the trap column and sequentially to the analytical column using a gradient of 0-50% solvent B in solvent A over a period of 125 minutes [solvent A: 0.1% formic acid (FA), 2% acetonitrile; solvent D: 0.1% FA, 70% acetonitrile), then 50-100% solvent B for 10 minutes at a flow rate 200 nl/minute. The RP column eluate was analyzed using a Q-STAR ELITE mass spectrometer (Applied Biosystems Inc.) in information-dependent acquisition (IDA) mode with the scan cycles set to perform a 1-second MS scan followed by 3 MS/MS scans for 2 seconds each. The acquisition method was set to allow 1 repetition at any m/z, followed by dynamic exclusion for a period of 60 seconds. Relative protein abundance was determined using the results of MS/MS scans of the iTRAQ-labeled peptides. iTRAQ-labeled peptides were fragmented under collision-induced dissociation (CID) conditions to give fragment ions the sequence information for the peptide and reporter ions. Thus, the identity of the protein from which the peptide was analyzed was confirmed and the ratios of the peak areas of the iTRAQ reporter ions used to compare the relative abundance of the protein identified in the sample.

The software packages used for data acquisition and analysis were Analyst 1.1 and Protein Pilot 4.0, respectively. We searched the Ref-Seq human database provided by NCBI. The confidence score, based on a Protein Pilot generated value, was used to evaluate the quality of the sequence of the identified peptide. For each patient, we selected proteins based on the relative expression in PDAC tissue as compared with pooled MPD that was greater than the average ratio +2 SD,

then evaluated the frequency of the selected proteins in the 7 PDAC patients.

Antibodies

Anti-DPYSL3 was purchased from Millipore (Billerica, MA), pY397-FAK from Abcam (Cambridge, MA), anti-PARP, anti-caspase-8, and anti-Erk from Cell Signaling Technology (Beverly, MA), anti-Lamin and anti-c-myc from Santa Cruz Biotechnology (Santa Cruz, CA), and anti-α-tubulin, anti-β-actin, anti-vinculin, and agarose-conjugated anti-c-myc from Sigma-Aldrich (St Louis, MO).

Plasmid construction and transfection, and establishment of stable clones

The full length DPYSL3 open reading frame (IMAGE clone 6177053) was obtained from Invitrogen (Carlsberg, CA) and a 4710-bp EcoRI fragment containing the entire coding sequence of DPYSL3 was cloned into pcDNA3 (pcDNA3-DPYSL3). For construction of myc-tagged DPYSL3, a 2052-bp open reading frame was amplified using myc-tag containing a primer and the resultant product was cloned into pcDNA3 (pcDNA3-myc-DPYSL3). Sequence confirmation was conducted thoroughly. PANC-1 cells were transfected with pcDNA3-DPYSL3 or pcDNA3 plasmid using Fugene 6 reagent (Roche, Alameda, CA), according to the manufacturer's instructions, and selected with the aid of 600 μg/ml of neomycin for 2 weeks to establish stable clones (PANC-1-DPYSL3 #1 and #2, and Panc-1-VC #1 and #2). PANC-1 cells were also transfected with a pcDNA3-DPYSL3-myc or pcDNA3-myc plasmid using Fugene 6 reagent, then selected with the aid of 600 μg/ml of neomycin for 2 weeks to establish stable clones (PANC-1-DPYSL3-myc, PANC-1-VC-myc). The expression of DPYSL3 was confirmed based on western blotting findings.

Western blot analysis, colorimetric analysis, and flow cytometric analysis

At 24 hours before transfection of siRNAs, 1×10^5 of CFPAC-1 cells were plated. Knockdown of DPYSL3 was carried out by transfection of 20 nM of siRNA targeting DPYSL3 (two Mission siRNAs: SASI_Hs01_00065697 and SASI_Hs01_00065698, Sigma-Aldrich, St Louis, MO) using RNAi-MAX (Invitrogen), according to the manufacturer's instructions, with culture media replaced at 24 hours after transfection. Cells were harvested with SDS-sample buffer at 96 hours after transfection and subjected to western blot analysis, and the numbers of viable cells were determined with TetraColor One (Seikagaku, Tokyo, Japan) at 48 hours after transfection. Lysates from CFPAC-1 and SU86.86 cells were treated with 0.2 unit/μl of alkaline phosphatase (TAKARA BIO Inc., Shiga, Japan) for 30 minutes at 37°C. CFPAC-1 and SU86.86 cells were treated with 0.1μg/ml of tunicamycin (glycosylation inhibitor, SIGMA-Aldrich) for 8 hours and then harvested with SDS-sample buffer. Total cell lysates (10 μg) were separated using SDS-PAGE and transferred to membranes. Western blotting results were quantitated using Image J software (http://rsb.info.nih.gov/ij/index.html), according to the instructions. The ratio of expressions of DPYSL3 and β-actin was calculated, then used for comparison of the expression level of DPYSL3 in PDAC patients. Those patients with a ratio higher than average were determined to be high expressers. For flow cytometric analysis, transfected cells were harvested using 0.5% NP-40 at 48 hours after transfection, then cell nuclei were stained with propidium iodide (Sigma-Aldrich) and cellular DNA contents measured using a FACScalibur flow cytometer equipped with the CELLQuest program (BD Biosciences, Bedford, MA). Analyses of induction of apoptosis were conducted using an annexin V-FITC staining kit (BD Biosciences). Attached and/or floating cells were collected at 48 hours after transfection, and stained with annexin V-FITC, following the manufacturer's instructions. At least 3 independent experiments using colorimetric and flow cytometric assays were performed.

Adhesion assay

Cells were serum-starved overnight, then resuspended in serum-free DMEM/0.1% BSA and incubated in suspension for 3 hours at 37°C. Six-well plates were coated with 10 μg/ml fibronectin/PBS overnight at room temperature, then washed twice and dried. Next, 3×10^4 of Panc-1-DPYSL3 or -VC cells were seeded onto the plates and incubated for 1 hour at 37°C in a CO_2 incubator. The plates were shaken for 60 seconds at 60 rpm twice, and floating cells were removed using 2 wash cycles with PBS. Adherent cells were collected and counted using a Coulter Counter, or lysed with SDS-sample buffer for western blot analysis. Three independent experiments were performed in triplicate.

Quantitative real-time RT-PCR

Total RNA samples were prepared from MIA PaCa-2, PANC-1, SW 1990, Capan-1, CFPAC-1, SU86.86, Hs766T and ACBRI515 using an RNeasy Mini Kit (QIAGEN, Valencia, CA). Complementary DNA samples were prepared using a High-Capacity cDNA Reverse Transcription Kit (Applied Biosystems Inc.). A TaqMan PCR assay was also performed to quantify DPYSL3 mRNA expression using commercially available FAM™-labeled probes for DPYSL3 and VIC™-labeled probes for 18S, according to the manufacturer's instructions. Ct values for DPYSL3 were normalized to those of 18S (ΔCt). The average ΔΔCt values were then calculated after normalization to the ΔCt value obtained at time point 0.

Immunofluorescence analysis

Panc-1-DPYSL3 or -VC cells (4×10^4) were transferred to cover glasses coated with fibronectin (5 μg/ml PBS), and cultured for 12 hours. The cells were fixed in 3.7% formaldehyde for 10 minutes, treated with PBS containing 0.3% Triton X-100 for 5 minutes, and incubated with anti-vinculin antibody for 1 hour at room temperature. Cells were then washed 3 times with PBS, incubated for 1 hour with Alexa 488-conjugated secondary antibody (Molecular Probes, Carlsberg, CA), and analyzed using a fluorescent microscope.

In-vivo metastasis assay

An experimental metastasis assay following tail vein injection of tumor cells was performed, essentially as described by [14].

CFPAC-1 cells and NCI-H460-LNM35 cells were transfected with either siControl or siDPYSL3 #1 as described above, then the transfectants were labeled with calcein (BD Biosciences) for one hour at 24 hours after siRNA transefection. Labeled cells were collected and counted, and 1.0 x 10^6 cells in 0.1 ml of PBS were injected into tail veins of 6-week-old female SCID mice. Two days after injection, the mice were euthanized, then 6ml of PBS was injected into the right ventricle for perfusion of the lung microvasculature. The perfused lungs were embedded in OCT (Sakura), sectioned (thickness 10 mm) with a Leica CM3050 (Leica Microsystems), and fixed using Fluoromount. Perfusion-resistant cells were determined by direct counting in the sections using an A1 Rsi confocal microscope. Five thin slices were obtained from each mouse lung specimen and images (x20) of each slice were obtained. The number of fluorescent-positive cancer cells was counted and determined for each mouse, and then the average value for each treatment was calculated.

Identification of DPYSL3 and DPYSL3-bound proteins in pancreatic cancer cells

GST-tagged DPYSL3 proteins were expressed in Sf9 insect cells using a Gateway system (Invitrogen), according to the manufacturer's instructions. GST-tagged DPYSL3 proteins were purified using glutathione-sepharose (GE Healthcare, Waukesha, WI), then mixed with a protein extract from CFPAC-1 cells. DPYSL3-bounded proteins were eluted by addition of 2 mM of glutathione, and reduced, alkylated, and digested with trypsin according to the manufacturer's instructions (Applied Biosystems Inc.). Further peptide sequence analyses were conducted by mass spectrometry (Thermo Fisher Scientific, Waltham, MA). Transitions for MRM analyses were created with MRM pilot v2.0 according to the manufacturer's instructions (Applied Biosystems Inc.) using peptide information obtained from sequence analyses of candidate DPYSL3-bounded proteins. An MRM run was performed for the predetermined transitions using a 4000 Q TRAP hybrid triple quadrupole/linear ion trap instrument (AB Sciex, Foster City, CA) in MRM mode. Multiple peptides per candidate protein (at least two peptides for each) and three transition peptides were used. Aliquots (up to 10 µg) of freshly prepared test (purified from a mixture of CFPAC-1 cell lysate, GST-DPYSL3, and glutathione-beads) and negative control (purified from a mixture of CFPAC-1 cell lysate, purified GST protein, and glutathione-beads) samples as well as SU86.86 cell lysate were reduced, alkylated, and digested with trypsin according to the manufacturer's instructions (Applied Biosystems Inc.). Digested peptide samples were injected into a reverse-phase (RP) trap column (HiQ Sil C18-3, 0.8-mm i.d. x 3 mm) and then separated with an RP analytical column (HiQ Sil C18-3 Gradient, 0.15-mm i.d. x 50 mm) using a gradient of 0-50% solvent B in solvent A over a period of 125 minutes [solvent A: 0.1% formic acid (FA), 2% acetonitrile; solvent D: 0.1% FA, 70% acetonitrile) followed by 50-100% solvent B for 10 minutes at a flow rate 200 nl/minute. MRM transitions were acquired at unit resolution in both Q1 and Q3 quadrupoles to maximize specificity. The scan time was maintained at 50 ms for each transition, and the pause time between transition scans was set to 5 ms. Once electrospray MS data were collected, then the peaks were integrated using quantitation procedures in the Analyst software 1.4.2 (Intelli-Quan algorithm).

Immunoprecipitation and pulldown assay

After an overnight culture, 6×10^5 of Panc-1-pcDNA3-DPYSL3-myc or pcDNA3-myc cells were lysed in 1 ml of NP-40 lysis buffer (20 mM Tris-HCl pH 8.0, 100 mM NaCl, 0.5% NP-40, 5 mM EDTA) supplemented with protease inhibitor and centrifuged at 15,000 rpm at 4°C for 30 minutes. Next, 300 µl of supernatant was transferred to new tubes and incubated with the anti-Ezrin antibody overnight at 4°C. Protein G-sepharose beads (GE Healthcare) were added to the solutions and incubated for 2 hours at 4°C. Immunoprecipitates were extensively washed 4 times and the eluted precipitates were resolved using SDS-PAGE. For pull-down precipitation assays, 300 µl of supernatant from the lysate of PANC-1-pcDNA3-DPYSL3-myc or pcDNA3-myc cells was incubated overnight at 4°C with 15 µl of agarose-conjugated anti-c-myc antibody. Immunoprecipitates were extensively washed 4 times and the eluted precipitates were resolved using SDS-PAGE.

Supporting Information

Figure S1. Detection of DPYSL3 transcripts by quantitative real-time PCR and analyses of modification of DPYSL3 protein western blot analyses in pancreatic cancer cell lines. (A) Total RNA samples were extracted from each cells. Complementary DNA samples were prepared using a High-Capacity cDNA Reverse Transcription Kit (Applied Biosystems Inc.) were subjected using TaqMan probe (Applied Biosystems Inc.). Value of ACBRI515, normal pancreatic cell line, set as 1. Error bars denote SD. (B) Lysates from CFPAC-1 and SU86.86 cells were treated with 0.2 unit/µl of alkaline phosphatase for 30 minutes at 37°C. CFPAC-1 and SU86.86 cells were treated with 0.1µg/ml of tunicamycin (glycosylation inhibitor) for 8 hours and then harvested with SDS-sample buffer. Total cell lysates were separated using SDS-PAGE and transferred to membranes.
(TIF)

Figure S2. DPYSL3 protein expression in SU86.86 pancreatic cancer cell lines. MRM analyses using four additional transitions revealed that DPYSL3 existed in a SU86.86 cell line. SU86.86 cell lysates were reduced, alkylated, and digested with trypsin and the analyzed by a 4000 Q TRAP hybrid triple quadrupole/linear ion trap instrument.
(TIF)

Figure S3. siDPYSL3 treatment in DPYSL3 negative pancreatic cancer cell lines, MIA PaCa-2 and PANC-1. siRNA against DPYSL3 showed no effect on cell viability. Data are shown as the mean ± SD (n=3).
(TIF)

Figure S4. DPYSL3 knockdown reduces cell adhesion of pancreatic cancer cell line, CFPAC-1. Phase contrast micrographs of CFPAC-1 pancreatic cancer cell linesobtained 3 days after siRNA transfection. Marked number of cells were detached from bottom of dish. Lower panels are magnified images of those in upper panel. Arrow head, representative floating cells. Arrow, attached cells. Scale bar, 50 μm.
(TIF)

Figure S5. DPYSL3 expression in NCI-H460-LNM35 cells. (A) Higher expression of DPYSL3 was observed in highly metastatic NCI-H460-LNM35 compared to low metastatic parental cell line, NCI-H460-N15. (B) Treatment with siDPYSL3 markedly reduced expression of DPYSL3 . (C) Introduction of siDPYSL3 markedly reduced migration ability in NCI-H460-LNM35 cells. Lower panels show magnified images. (D) Experimental metastasis assay of NCI-H460-LNM35 cells knocked down for DPYSL3 with siDPYSL3 #1 (five mice per treatment). Five thin slices were obtained from lung specimen of each mouse and x20 image was obtained from each slice. The number of fluorescent label positive cancer cells were counted and average value was calculated in each mice. Data are shown as the mean ± SD (n=5). *p < 0.001 versus siControl as determined by Student's t test. (E) Representative fluorescence images of perfusion-resistant cells. Cells were stained with calcein. Bars indicate 20 μm.
(TIF)

Figure S6. Identification of binding partner of DPYSL3. (A) Workflow for proteomic identification and confirmation of DPYSL3 binding proteins in pancreatic cancer cell line. (B) MRM confirmation of candidate proteins supposed to interact with DPYSL3 were identified from MSMS analyses. Interaction between DPYSL3 and EZR protein was validated. (C) Significant interactions between DPYSL3 and some of the candidates were not confirmed in the test sample (CFPAC-1 cell lysate and GST-DPYSL3), nor in the control samples (CFPAC-1 cell lysate and purified GST).
(TIF)

Table S1. Clinicopathologic characteristics of patients with pancreatic cancer in the discovery cohort.
(DOCX)

Table S2. Clinicopathologic characteristics of patients with pancreatic cancer in the validation cohort.
(DOCX)

Table S3. (XLSX)

Table S4. MRM transitions for confirmation of DPYSL3 interacting proteins.
(DOCX)

Author Contributions

Conceived and designed the experiments: TT KY. Performed the experiments: TK NH YO KY SK KK. Analyzed the data: YO KY. Contributed reagents/materials/analysis tools: YY MN. Wrote the manuscript: TT KY.

References

1. Cancer statistics. Available: http://ganjoho.jp/data/professional/statistics/backnumber/2010/fig01.pdf. Accessed 2013 Oct 31.)
2. Giaccone G (2002) Clinical impact of novel treatment strategies. Oncogene 21: 6970-6981. doi:10.1038/sj.onc.1205565. PubMed: 12362278.
3. Tomida S, Takeuchi T, Shimada Y, Arima C, Matsuo K et al. (2009) Relapse-related molecular signature in lung adenocarcinomas identifies patients with dismal prognosis. J Clin Oncol 27: 2793-2799. doi: 10.1200/JCO.2008.19.7053. PubMed: 19414676.
4. Tomida S, Yanagisawa K, Koshikawa K, Yatabe Y, Mitsudomi T et al. (2007) Identification of a metastasis signature and the DLX4 homeobox protein as a regulator of metastasis by combined transcriptome approach. Oncogene 26: 4600-4608. doi:10.1038/sj.onc.1210242. PubMed: 17260014.
5. Takeuchi T, Tomida S, Yatabe Y, Kosaka T, Osada H et al. (2006) Expression profile-defined classification of lung adenocarcinoma shows close relationship with underlying major genetic changes and clinicopathologic behaviors. J Clin Oncol 24: 1679-1688. doi:10.1200/JCO.2005.03.8224. PubMed: 16549822.
6. Koshikawa K, Osada H, Kozaki K, Konishi H, Masuda A et al. (2002) Significant up-regulation of a novel gene, CLCP1, in a highly metastatic lung cancer subline as well as in lung cancers in vivo. Oncogene 21: 2822-2828. doi:10.1038/sj.onc.1205405. PubMed: 11973641.
7. Kozaki K, Koshikawa K, Tatematsu Y, Miyaishi O, Saito H et al. (2001) Multi-faceted analyses of a highly metastatic human lung cancer cell line NCI-H460-LNM35 suggest mimicry of inflammatory cells in metastasis. Oncogene 20: 4228-4234. doi:10.1038/sj.onc.1204561. PubMed: 11464289.
8. Kozaki K, Miyaishi O, Tsukamoto T, Tatematsu Y, Hida T et al. (2000) Establishment and characterization of a human lung cancer cell line NCI-H460-LNM35 with consistent lymphogenous metastasis via both subcutaneous and orthotopic propagation. Cancer Res 60: 2535-2540. PubMed: 10811136.
9. Yanagisawa K, Shyr Y, Xu BJ, Massion PP, Larsen PH et al. (2003) Proteomic patterns of tumour subsets in non-small-cell lung cancer. Lancet 362: 433-439. doi:10.1016/S0140-6736(03)14068-8. PubMed: 12927430.
10. Yanagisawa K, Tomida S, Shimada Y, Yatabe Y, Mitsudomi T et al. (2007) A 25-signal proteomic signature and outcome for patients with resected non-small-cell lung cancer. J Natl Cancer Inst 99: 858-867. doi:10.1093/jnci/djk197. PubMed: 17551146.
11. Yanagisawa K, Konishi H, Arima C, Tomida S, Takeuchi T et al. (2010) Novel metastasis-related gene CIM functions in the regulation of multiple cellular stress-response pathways. Cancer Res 70: 9949-9958. doi:10.1158/0008-5472.CAN-10-1055. PubMed: 21118962.
12. Turtoi A, Musmeci D, Wang Y, Dumont B, Somja J et al. (2011) Identification of novel accessible proteins bearing diagnostic and therapeutic potential in human pancreatic ductal adenocarcinoma. J Proteome Res 10: 4302-4313. doi:10.1021/pr200527z. PubMed: 21755970.
13. Sun C, Rosendahl AH, Ansari D, Andersson R (2011) Proteome-based biomarkers in pancreatic cancer. World J Gastroenterol 17: 4845-4852. doi:10.3748/wjg.v17.i44.4845. PubMed: 22171124.
14. Shibue T, Weinberg RA (2009) Integrin beta1-focal adhesion kinase signaling directs the proliferation of metastatic cancer cells disseminated in the lungs. Proc Natl Acad Sci U S A 106: 10290-10295. doi:10.1073/pnas.0904227106. PubMed: 19502425.
15. Medina R, Ghule PN, Cruzat F, Barutcu AR, Montecino M et al. (2012) Epigenetic control of cell cycle-dependent histone gene expression is a principal component of the abbreviated pluripotent cell cycle. Mol Cell Biol 32: 3860-3871. doi:10.1128/MCB.00736-12. PubMed: 22826438.
16. Ketterer B (2001) A bird's eye view of the glutathione transferase field. Chem Biol Interact 138: 27-42. doi:10.1016/S0009-2797(01)00277-0. PubMed: 11640913.
17. Fehon RG, McClatchey AI, Bretscher A (2010) Organizing the cell cortex: the role of ERM proteins. Nat Rev Mol Cell Biol 11: 276-287. doi:10.1038/nrm2866. PubMed: 20308985.

18. Frame MC, Patel H, Serrels B, Lietha D, Eck MJ (2010) The FERM domain: organizing the structure and function of FAK. Nat Rev Mol Cell Biol 11: 802-814. doi:10.1038/nrm2996. PubMed: 20966971.
19. Srivastava J, Elliott BE, Louvard D, Arpin M (2005) Src-dependent ezrin phosphorylation in adhesion-mediated signaling. Mol Biol Cell 16: 1481-1490. doi:10.1091/mbc.E04-08-0721. PubMed: 15647376.
20. Steeg PS (2003) Metastasis suppressors alter the signal transduction of cancer cells. Nat Rev Cancer 3: 55-63. doi:10.1038/nrc967. PubMed: 12509767.
21. Hanash S (2003) Disease proteomics. Nature 422: 226-232. doi: 10.1038/nature01514. PubMed: 12634796.
22. Goshima Y, Nakamura F, Strittmatter P, Strittmatter SM (1995) Collapsin-induced growth cone collapse mediated by an intracellular protein related to UNC-33. Nature 376: 509-514. doi: 10.1038/376509a0. PubMed: 7637782.
23. Gaetano C, Matsuo T, Thiele CJ (1997) Identification and characterization of a retinoic acid-regulated human homologue of the unc-33-like phosphoprotein gene (hUlip) from neuroblastoma cells. J Biol Chem 272: 12195-12201. doi:10.1074/jbc.272.18.12195. PubMed: 9115293.
24. Fukada M, Watakabe I, Yuasa-Kawada J, Kawachi H, Kuroiwa A et al. (2000) Molecular characterization of CRMP5, a novel member of the collapsin response mediator protein family. J Biol Chem 275: 37957-37965. doi:10.1074/jbc.M003277200. PubMed: 10956643.
25. Wang LH, Strittmatter SM (1997) Brain CRMP forms heterotetramers similar to liver dihydropyrimidinase. J Neurochem 69: 2261-2269. PubMed: 9375656.
26. Arimura N, Inagaki N, Chihara K, Ménager C, Nakamura N et al. (2000) Phosphorylation of collapsin response mediator protein-2 by Rho-kinase. Evidence for two separate signaling pathways for growth cone collapse. J Biol Chem 275: 23973-23980. doi:10.1074/jbc.M001032200. PubMed: 10818093.
27. Shih JY, Lee YC, Yang SC, Hong TM, Huang CY et al. (2003) Collapsin response mediator protein-1: a novel invasion-suppressor gene. Clin Exp Metastasis 20: 69-76. doi:10.1023/A:1022598604565. PubMed: 12650609.
28. Shih JY, Yang SC, Hong TM, Yuan A, Chen JJ et al. (2001) Collapsin response mediator protein-1 and the invasion and metastasis of cancer cells. J Natl Cancer Inst 93: 1392-1400. doi:10.1093/jnci/93.18.1392. PubMed: 11562390.
29. Dong J, Hu Z, Wu C, Guo H, Zhou B et al. Association analyses identify multiple new lung cancer susceptibility loci and their interactions with smoking in the Chinese population. Nat Genet.

Cell PRESS

Cancer Cell

Minireview

NKX2-1/TTF-1: An Enigmatic Oncogene that Functions as a Double-Edged Sword for Cancer Cell Survival and Progression

Tomoya Yamaguchi,[1] Yasuyuki Hosono,[1] Kiyoshi Yanagisawa,[1] and Takashi Takahashi[1,*]

[1]Division of Molecular Carcinogenesis, Center for Neurological Diseases and Cancer, Nagoya University Graduate School of Medicine, Nagoya 466-8550, Japan

*Correspondence: tak@med.nagoya-u.ac.jp

http://dx.doi.org/10.1016/j.ccr.2013.04.002

Emerging evidence indicates that NKX2-1, a homeobox-containing transcription factor also known as TTF-1, plays a role as a "lineage-survival" oncogene in lung adenocarcinomas. In T cell acute lymphoblastic leukemia, gene rearrangements lead to aberrant expression of NKX2-1/TTF-1. Despite accumulating evidence supporting its oncogenic role, it has become apparent that NKX2-1/TTF-1 expression also has biological and clinical functions in the opposite direction that act against tumor progression. Herein, we review recent findings showing these enigmatic double-edged characteristics, with special attention given to the roles of NKX2-1/TTF-1 in lung development and carcinogenesis.

Oncogenic Involvement of NKX2-1/TTF-1

Emerging evidence suggests that "lineage-specific addiction" to survival mechanisms that are programmed for developmental roles in normal progenitor cells of particular lineages may exist in cancer cells. The transcription factor MITF in melanoma is considered to be an archetypal prototype (Garraway and Sellers, 2006), whereas survival of lung cancers with neuroendocrine (NE) features such as small-cell lung cancer (SCLC) is dependent on continued expression of ASH1, a transcription factor indispensable for pulmonary NE cell development (Nishikawa et al., 2011; Osada et al., 2005, 2008). Thyroid transcription factor 1 (TTF-1), also known as NKX2-1, is a homeobox-containing transcription factor essential for the development of the lung and thyroid as well as a restricted part of the brain (Stanfel et al., 2005), and a series of peripheral lung cells defined as the terminal respiratory unit (TRU) is under the control of this master regulator. About 70% of adenocarcinomas express NKX2-1/TTF-1 independent of disease stage and retain features of the TRU to a certain extent (Yatabe et al., 2002). These TRU-type adenocarcinomas exhibit a distinctively higher prevalence of *EGFR* mutations, disproportionately high occurrence in females and nonsmokers, and characteristic expression profiles; in fact, *p53* and *KRAS* mutations are inversely associated with NKX2-1/TTF-1 expression (Takeuchi et al., 2006; Yatabe et al., 2005). We and others have previously found that NKX2-1/TTF-1-positive lung adenocarcinomas are dependent on sustained expression of NKX2-1/TTF-1 and sometimes even exhibit focal copy-number increases (Figure 1; Table 1) (Kendall et al., 2007; Kwei et al., 2008; Tanaka et al., 2007; Weir et al., 2007). Intriguingly, *Nkx2-1/Ttf-1* transgenic mice exhibit hyperplasia of type II alveolar cells (Wert et al., 2002). In addition, NKX2-1/TTF-1 is prominently expressed in lung epithelial cells undergoing regeneration (Stahlman et al., 1996). Furthermore, haploinsufficiency of *Nkx2-1/Ttf-1* was recently reported to reduce tumor formation in transgenic mice expressing mutant EGFR (Maeda et al., 2012).

Several lines of evidence suggest possible oncogenic involvement of *NKX2-1/TTF-1* in other types of cancers. In addition to the lung, the thyroid is another organ that expresses NKX2-1/TTF-1. A germline missense mutation of *NKX2-1/TTF-1* that results in a valine substitution for alanine at codon 339 has been identified in families affected by multinodular goiter and papillary thyroid carcinoma (Ngan et al., 2009). It is of note that the SNP rs944289, which maps close to *NKX2-1/TTF-1*, was shown to be significantly associated with increased risk of thyroid cancer (Gudmundsson et al., 2009), although the mechanistic link remains to be elucidated. Rearrangements of *NKX2-1/TTF-1* with T cell receptor or immunoglobulin heavy-chain loci were recently identified in T cell acute lymphoblastic leukemia (T-ALL), suggesting a role in the pathogenesis of hematopoietic malignancies (Homminga et al., 2011). Rearrangements and ectopic expression of *NKX2-2* and *NKX2-5*, both homeobox-containing transcription factors closely related to *NKX2-1/TTF-1*, have also been reported in a subset of T-ALL (Homminga et al., 2011; Nagel et al., 2003). These data strongly suggest an oncogenic role for NKX2-1/TTF-1 as well as other members of the NK2 family, not only in lung and thyroid cancers but also in hematopoietic malignancies. On the other hand, *NKX2-8*, residing in close proximity to *NKX2-1*, exhibits loss of heterozygosity and reduced expression in lung squamous cell carcinomas (Harris et al., 2011), suggesting distinct modes of involvement.

Enigma Surrounding NKX2-1/TTF-1 in Tumor Biology

Despite its role as a lineage-survival oncogene in lung adenocarcinomas, NKX2-1/TTF-1 expression is also known to be associated with favorable prognosis in affected patients (Anagnostou et al., 2009). Evidence to explain this paradox has recently emerged (Figure 2). For example, we found that *MYBPH* is directly transactivated by NKX2-1/TTF-1 and inhibits phosphorylation of the myosin regulatory light chain via direct interaction with ROCK1, which is a prerequisite process for acquisition of assembly competence (Hosono et al., 2012b). In addition, MYBPH directly binds to and inhibits assembly of nonmuscle myosin heavy chain IIA (Hosono et al., 2012a), thereby conferring

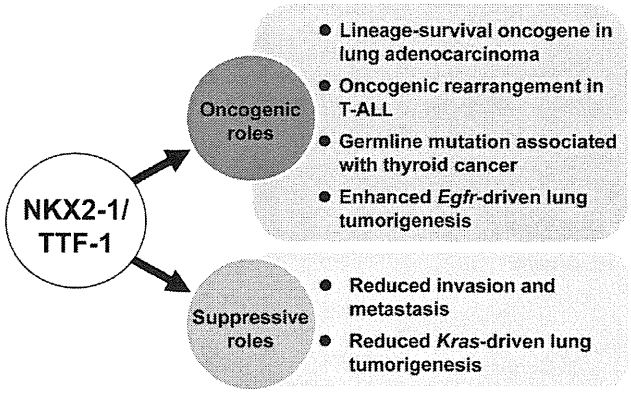

Figure 1. Double-Edged Characteristic of NKX2-1/TTF-1
NKX2-1/TTF-1 has shown both oncogenic and inhibitory activities in cancer development and progression.

firm inhibition of actomyosin assembly by two distinct mechanisms and consequently reducing cell motility, invasion, and metastasis. These apparently deleterious effects in lung adenocarcinoma progression appear to be negated by frequent promoter DNA methylation of *MYBPH*. The epithelial tight-junction protein OCLN as well as two other epithelial tight-junction proteins, CLDN1 and CLDN18, were also shown to be transcriptionally activated by NKX2-1/TTF-1 (Niimi et al., 2001; Runkle et al., 2012). These findings indicate that genes implicated in regulation of cytoskeletal and cell-cell organization are prime transcriptional targets of TTF-1, which negatively affects cell motility, invasion, and metastasis and is also conceivably involved in lung morphogenesis and regeneration after lung injury. In addition, downregulation of *Nkx2-1/Ttf-1* has been shown to lead to eventual derepression of *Hmga2* and acquisition of metastatic ability in a mouse model of lung adenocarcinoma with conditionally activated *Kras* and loss-of-function *p53* mutant alleles (Snyder et al., 2013; Winslow et al., 2011). Interestingly, haploinsufficiency or conditional knockout of *Nkx2-1/Ttf-1* was recently reported to enhance development of invasive *Kras*-driven mucinous lung adenocarcinoma (Maeda et al., 2012; Snyder et al., 2013), in contrast to suppressing *Egfr*-driven lung tumorigenesis (Maeda et al., 2012). Loss of Nkx2-1/Ttf-1 appears to induce the mucin-producing phenotype through consequential release of Foxa1/Foxa2, transcription factors known to physically interact and cooperate with Nkx2-1/Ttf-1, onto de novo binding sites near gastrointestinal differentiation-related genes including Hnf4α, which critically regulates the differentiation program (Snyder et al., 2013). Along this line, it is notable that human invasive mucinous adenocarcinomas of the lung almost invariably express HNF4α, and have exhibited a significant association with negative TTF-1 expression and positive KRAS mutation status (Kunii et al., 2011). Although epithelial-to-mesenchymal transition (EMT) is linked with cancer progression, NKX2-1/TTF-1 represses TGF-β-induced EMT by alleviating TGF-β-mediated induction of Snail and Slug, as well as by reducing TGF-β production (Saito et al., 2009). Conversely, TGF-β represses NKX2-1/TTF-1 by induction of miR-365 (Qi et al., 2012). Thus, accumulated evidence points to the notion that NKX2-1/TTF-1 plays a double-edged role in cancer.

NKX2-1/TTF-1-Mediated Lineage-Survival Signaling

Despite the requirement for sustained NKX2-1/TTF-1 expression in the survival of lung adenocarcinoma cells, NKX2-1/TTF-1 itself cannot be considered as a molecular target for treating this devastating cancer because of its indispensable roles in normal lung physiology, such as the production and secretion of surfactant proteins. Thus, elucidation of how NKX2-1/TTF-1 mediates survival signals has long been anticipated. In this regard, we recently found that NKX2-1/TTF-1 directly transactivates the receptor tyrosine kinase *ROR1*, which in turn sustains a favorable balance between prosurvival PI3K-AKT and proapoptotic p38 signaling, in part through ROR1 kinase-dependent c-Src activation as well as kinase activity-independent sustainment of EGFR-ERBB3 association, ERBB3 phosphorylation, and consequential PI3K activation (Yamaguchi et al., 2012). These findings may underlie the molecular basis for the functional interrelationship between NKX2-1/TTF-1 and EGFR. Consistently, NKX2-1/TTF-1 expression is significantly associated with *EGFR* mutations in lung cancer tissues (Takeuchi et al., 2006; Yatabe et al., 2005), and *Nkx2-1/Ttf-1* haploinsufficiency reduces mutant *Egfr*-driven lung tumorigenesis (Maeda et al., 2012). It is also of particular interest from a clinical point of view that ROR1 inhibition appears to be effective for treatment of lung adenocarcinomas carrying various gefitinib-resistance mechanisms, such as secondary EGFR mutations and HGF overexpression, because the existence of such diverse mechanisms makes it difficult to predict which should be targeted to prevent expansion of resistant clones. This molecule with possible druggability, namely a cell-surface receptor with a

Table 1. Alterations of the NK2 Family in Human Cancers

NK2 Family	Aberrations	Organ Sites	Cancer Types	References
NKX2-1	amplification	lung	adenocarcinoma	Tanaka et al., 2007
	amplification	lung	adenocarcinoma	Kendall et al., 2007
	amplification	lung	adenocarcinoma	Weir et al., 2007
	amplification	lung	adenocarcinoma	Kwei et al., 2008
	germline mutation	thyroid	multinodular goiter, papillary adenocarcinoma	Ngan et al., 2009
	rearrangement	hematopoietic	T cell acute lymphoblastic leukemia	Homminga et al., 2011
NKX2-2	rearrangement	hematopoietic	T cell acute lymphoblastic leukemia	Homminga et al., 2011
NKX2-5	rearrangement	hematopoietic	T cell acute lymphoblastic leukemia	Nagel et al., 2003
NKX2-8	loss of heterozygosity	lung	squamous cell carcinoma	Harris et al., 2011

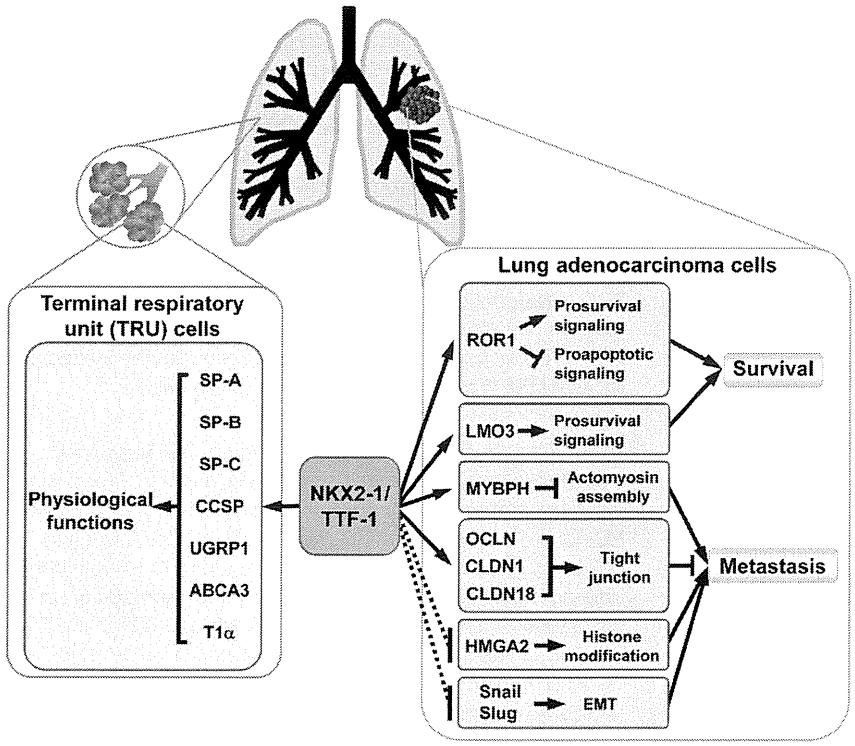

Figure 2. NKX2-1/TTF-1-Mediated Transcriptional Regulation and Consequences in Normal and Cancer Cells of the Lung

NKX2-1/TTF-1 is required for maintenance of physiological lung functions in addition to its developmental roles. The oncogene plays a role as a lineage-survival oncogene in lung adenocarcinomas, whereas it also inhibits invasion, metastasis, and progression, paradoxically conferring better prognosis. Solid and dashed lines represent direct and indirect regulation, respectively.

tyrosine kinase domain, may thus be considered to be an "Achilles' heel" in lung adenocarcinomas, and future development of therapeutic means is greatly anticipated to reduce the intolerable death toll from currently "hard-to-cure" lung adenocarcinomas. In addition to *ROR1*, *LMO3*, a paralog of the *LMO1* and *LMO2* oncogenes in T-ALL, was recently identified as an additional direct transcriptional target for mediating survival signals (Watanabe et al., 2013). NKX2-1/TTF-1 appears to cooperatively transactivate *LMO3* together with FOXA1, whereas *LMO3* knockdown induced apoptosis in a lung adenocarcinoma cell line. However, ectopic overexpression of *LMO3* failed to overcome *NKX2-1/TTF-1* knockdown-induced apoptosis, suggesting the existence of additional crucial targets for lineage-survival signaling in lung adenocarcinoma cells.

Developmental Roles of NKX2-1/TTF-1 in Relation to Cancer Biology

During embryonic lung development, temporal-spatial expression of NKX2-1/TTF-1 is tightly regulated. NKX2-1/TTF-1 expression is first detected in the ventral foregut endoderm during a very early stage and then becomes abundantly expressed in virtually all cells in the progenitor of the trachea arising from the lung primordium. As subsequent branching morphogenesis proceeds, NKX2-1/TTF-1 expression is progressively restricted to distal airway cells and finally confined to epithelial cells in the TRU (Stahlman et al., 1996; Yatabe et al., 2002). A lung rudiment in *Nkx2-1/Ttf-1* knockout mice exhibited proximal, albeit abnormal, airway characteristics, suggesting its dispensable nature in specification of the lung primordium and proximal lung morphogenesis (Minoo et al., 1999). In contrast, this oncogene was shown to be strictly required for distal lung morphogenesis (Yuan et al., 2000). *NKX2-1/TTF-1* critically translates instructive morphogenic signals from the surrounding mesenchyme into transcriptional regulation of its targets, which are mediated by factors including fibroblast growth factors, Sonic hedgehog, and bone morphogenetic proteins. In humans, *NKX2-1/TTF-1* haploinsufficiency confers the rare autosomal-dominant disorder benign hereditary chorea as well as brain-lung-thyroid syndrome, which is manifested by chorea, hypothyroidism, and infantile respiratory distress (Inzelberg et al., 2011). Human *NKX2-1/TTF-1* haploinsufficiency might be associated with lung tumorigenesis in context-dependent and subtype-specific manners, as reported in mice (Maeda et al., 2012; Snyder et al., 2013). Unfortunately, no comprehensive epidemiologic data on the predisposition to lung cancers in affected individuals have been presented.

In addition to lung adenocarcinoma, it is interesting to note that NKX2-1/TTF-1 is frequently detected in SCLCs, which usually arise in the proximal airway, a region that normally lacks NKX2-1/TTF-1 expression. Because NKX2-1/TTF-1 expression is seen in the lung primordium, this phenomenon may reflect an atavistic, yet committed, state of SCLCs, which is consistent with its lack of expression in small-cell carcinomas arising from other organs, despite the similar characteristics of small and round morphology and NE properties. Future study comparing NKX2-1/TTF-1 target gene regulation between adenocarcinomas and those in small-cell carcinomas of various organs, including the adult and developing fetal lungs, would likely shed light on both similarities and distinctions with regard to its functional roles.

Regulation of NKX2-1/TTF-1 and Context Dependence

The 42 kD major isoform is encoded by mRNAs harboring exons 2 and 3, whereas the 44 kD minor isoform is encoded by all three exons (Figure 3). The proximal major promoter contains a TATA-like element and binding sites for FOXA1 (also known as HNF-3α), FOXA2 (HNF-3β), and GATA6, all of which are known to be crucially involved in lung development (Costa et al., 2001). The minor distal promoter is regulated by SP1 and SP3. NKX2-1/TTF-1 directly transactivates multiple genes implicated to have physiological lung functions, including SP-A, SP-B, SP-C, CCSP (also known as CC10, uteroglobin, or secretoglobin),

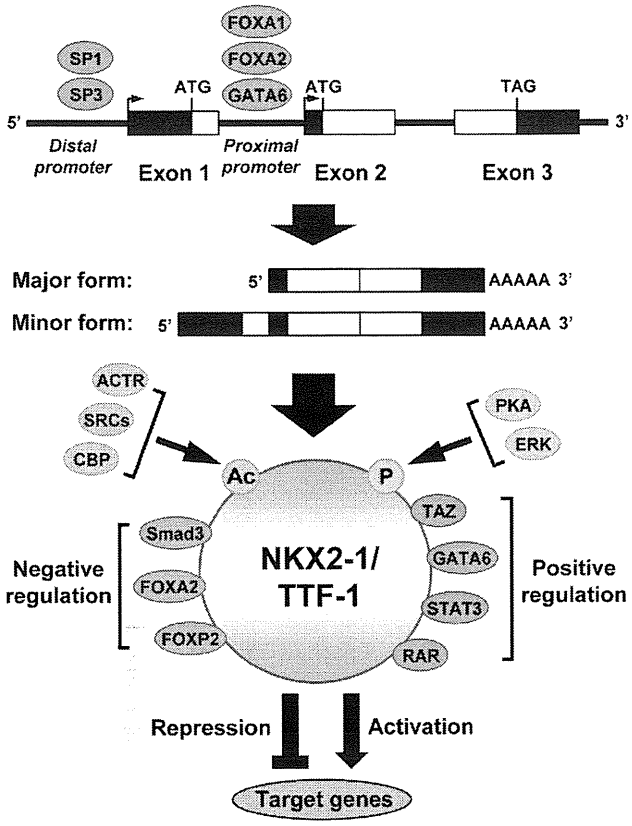

Figure 3. Regulatory Mechanisms of NKX2-1/TTF-1
NKX2-1/TTF-1 is transcribed from two distinct promoters under the influence of various transcription factors. Its transcriptional regulatory activities are modulated in a context-dependent manner, possibly by cooperating transcription factors as well as protein modifications. Ac, acetylation; P, phosphorylation.

UGRP1, and ABCA3. NKX2-1/TTF-1 also transactivates the functions of HOP, an HDAC-dependent negative regulator of NKX2-1/TTF-1 (Yin et al., 2006), as well as T1α, a type I pneumocyte-specific marker (Ramirez et al., 1997). CLDN18 and OCLN tight-junction proteins MYBPH, LMO3, and ROR1 have recently been identified as targets for their roles in cancer, as discussed above. Transcription factors that interact and cooperate with NKX2-1/TTF-1 include FOXA2 (Minoo et al., 2007), FOXP2 (Zhou et al., 2008), GATA6 (Liu et al., 2002), STAT3 (Yan et al., 2002), and RAR (Yan et al., 2001). Furthermore, Smad3 and TAZ modulate the transcriptional activity of NKX2-1/TTF-1 via their binding in a negative and positive manner, respectively (Li et al., 2002; Park et al., 2004). Posttranslational modifications are also important as a regulatory mechanism of NKX2-1/TTF-1 functions. Multiple nuclear coactivators, including ACTR, p160 steroid receptor coactivators, and p300/CBP, acetylate NKX2-1/TTF-1 (Yang et al., 2004), whereas NKX2-1/TTF-1 is also regulated through its phosphorylation, positively by PKA (Yan and Whitsett, 1997) and negatively by ERK (Missero et al., 2000). In addition, Smad3 physically interacts with NKX2-1/TTF-1 and inhibits NKX2-1/TTF-1-mediated transcription from the *SP-B* promoter lacking a Smad binding site (Li et al., 2002).

Recent ChIP-seq and ChIP-chip analyses have revealed a large number of additional potential transcriptional targets of NKX2-1/TTF-1 (Maeda et al., 2012; Tagne et al., 2012; Watanabe et al., 2013), with experimental validation of the induction of LMO3, E2F3, and cyclins B1 and B2, as well as repression of MUC5A, FGFR1, and MET. It is notable that NKX2-1/TTF-1 appears to be associated with and affect promoters via not only its canonical binding sites but also by the AP-1, forkhead, and nuclear hormone receptor-binding motifs. Therefore, downstream targets appear to be regulated by NKX2-1/TTF-1 in a context-dependent manner, possibly reflecting the expression of its cofactors.

Accumulating evidence, as noted above, implicates opposing roles of NKX2-1/TTF-1 in lung cancer development, which may also be the case in thyroid tumors and hematopoietic malignancies. NKX2-1/TTF-1 expression is absolutely required for peripheral lung development and differentiation, whereas its level in lung adenocarcinoma is associated with but not deterministic of differentiated morphologies (Takeuchi et al., 2006; Yatabe et al., 2002). It would be interesting to investigate whether any similarities and/or distinctions exist in the regulation of downstream targets by this enigmatic oncogene in cancer cells as well as in normal development, with special attention given to context dependence.

Conclusions and Future Perspectives

NKX2-1/TTF-1 has long been a focus of research in the field of lung and thyroid physiology, whereas emerging evidence has called attention to its roles in cancer. This oncogene appears to function as a double-edged sword in the pathogenesis of lung adenocarcinoma and possibly in other tumors as well. A future rigorous search for additional downstream molecules is warranted to gain a more complete picture of NKX2-1/TTF-1-centered regulatory networks in order to take advantage of its Jekyll-and-Hyde characteristics. It should also be kept in mind that current understanding of the regulatory web surrounding this enigmatic transcription factor may be oversimplified, as the same architecture may not exist in normal and cancerous states, or even among individual tumors. For example, a sizable fraction of NKX2-1/TTF-1-positive human lung adenocarcinomas are negative for surfactant proteins, which are authentic targets for transcriptional activation in normal lungs, and/or positive for HMGA2, a target for transcriptional repression. Opposing effects of *Nkx2-1/Ttf-1* haploinsufficiency in transgenic mice carrying mutant *Kras* and *Egfr* also suggest its multifaceted nature. Thus, the NKX2-1/TTF-1 regulatory networks present in cells in both normal and cancerous conditions may well be quite complex and context dependent, and likely require a radically different approach to elucidate. Along this line, a cancer systems biology approach with the aid of ever-increasing computing power may help to reveal a path to resolve this challenge, ultimately allowing an opportunity to take advantage of the double-edged characteristics of NKX2-1/TTF-1 in patients affected by cancer.

ACKNOWLEDGMENTS

We thank all of the members of our research group for their invaluable contributions, including helpful discussions and critical comments. We also

apologize for the incompleteness of the referencing due to space constraints. Studies in our laboratory have been supported in part by grants from the Ministry of Education, Science, Sports and Culture, Japan, and the Ministry of Health, Labor and Welfare, Japan.

REFERENCES

Anagnostou, V.K., Syrigos, K.N., Bepler, G., Homer, R.J., and Rimm, D.L. (2009). Thyroid transcription factor 1 is an independent prognostic factor for patients with stage I lung adenocarcinoma. J. Clin. Oncol. *27*, 271–278.

Costa, R.H., Kalinichenko, V.V., and Lim, L. (2001). Transcription factors in mouse lung development and function. Am. J. Physiol. Lung Cell. Mol. Physiol. *280*, L823–L838.

Garraway, L.A., and Sellers, W.R. (2006). Lineage dependency and lineage-survival oncogenes in human cancer. Nat. Rev. Cancer *6*, 593–602.

Gudmundsson, J., Sulem, P., Gudbjartsson, D.F., Jonasson, J.G., Sigurdsson, A., Bergthorsson, J.T., He, H., Blondal, T., Geller, F., Jakobsdottir, M., et al. (2009). Common variants on 9q22.33 and 14q13.3 predispose to thyroid cancer in European populations. Nat. Genet. *41*, 460–464.

Harris, T., Pan, Q., Sironi, J., Lutz, D., Tian, J., Sapkar, J., Perez-Soler, R., Keller, S., and Locker, J. (2011). Both gene amplification and allelic loss occur at 14q13.3 in lung cancer. Clin. Cancer Res. *17*, 690–699.

Homminga, I., Pieters, R., Langerak, A.W., de Rooi, J.J., Stubbs, A., Verstegen, M., Vuerhard, M., Buijs-Gladdines, J., Kooi, C., Klous, P., et al. (2011). Integrated transcript and genome analyses reveal NKX2-1 and MEF2C as potential oncogenes in T cell acute lymphoblastic leukemia. Cancer Cell *19*, 484–497.

Hosono, Y., Usukura, J., Yamaguchi, T., Yanagisawa, K., Suzuki, M., and Takahashi, T. (2012a). MYBPH inhibits NM IIA assembly via direct interaction with NMHC IIA and reduces cell motility. Biochem. Biophys. Res. Commun. *428*, 173–178.

Hosono, Y., Yamaguchi, T., Mizutani, E., Yanagisawa, K., Arima, C., Tomida, S., Shimada, Y., Hiraoka, M., Kato, S., Yokoi, K., et al. (2012b). MYBPH, a transcriptional target of TTF-1, inhibits ROCK1, and reduces cell motility and metastasis. EMBO J. *31*, 481–493.

Inzelberg, R., Weinberger, M., and Gak, E. (2011). Benign hereditary chorea: an update. Parkinsonism Relat. Disord. *17*, 301–307.

Kendall, J., Liu, Q., Bakleh, A., Krasnitz, A., Nguyen, K.C., Lakshmi, B., Gerald, W.L., Powers, S., and Mu, D. (2007). Oncogenic cooperation and coamplification of developmental transcription factor genes in lung cancer. Proc. Natl. Acad. Sci. USA *104*, 16663–16668.

Kunii, R., Jiang, S., Hasegawa, G., Yamamoto, T., Umezu, H., Watanabe, T., Tsuchida, M., Hashimoto, T., Hamakubo, T., Kodama, T., et al. (2011). The predominant expression of hepatocyte nuclear factor 4α (HNF4α) in thyroid transcription factor-1 (TTF-1)-negative pulmonary adenocarcinoma. Histopathology *58*, 467–476.

Kwei, K.A., Kim, Y.H., Girard, L., Kao, J., Pacyna-Gengelbach, M., Salari, K., Lee, J., Choi, Y.L., Sato, M., Wang, P., et al. (2008). Genomic profiling identifies TITF1 as a lineage-specific oncogene amplified in lung cancer. Oncogene *27*, 3635–3640.

Li, C., Zhu, N.L., Tan, R.C., Ballard, P.L., Derynck, R., and Minoo, P. (2002). Transforming growth factor-β inhibits pulmonary surfactant protein B gene transcription through SMAD3 interactions with NKX2.1 and HNF-3 transcription factors. J. Biol. Chem. *277*, 38399–38408.

Liu, C., Glasser, S.W., Wan, H., and Whitsett, J.A. (2002). GATA-6 and thyroid transcription factor-1 directly interact and regulate surfactant protein-C gene expression. J. Biol. Chem. *277*, 4519–4525.

Maeda, Y., Tsuchiya, T., Hao, H., Tompkins, D.H., Xu, Y., Mucenski, M.L., Du, L., Keiser, A.R., Fukazawa, T., Naomoto, Y., et al. (2012). Kras(G12D) and Nkx2-1 haploinsufficiency induce mucinous adenocarcinoma of the lung. J. Clin. Invest. *122*, 4388–4400.

Minoo, P., Su, G., Drum, H., Bringas, P., and Kimura, S. (1999). Defects in tracheoesophageal and lung morphogenesis in Nkx2.1(−/−) mouse embryos. Dev. Biol. *209*, 60–71.

Minoo, P., Hu, L., Xing, Y., Zhu, N.L., Chen, H., Li, M., Borok, Z., and Li, C. (2007). Physical and functional interactions between homeodomain NKX2.1 and winged helix/forkhead FOXA1 in lung epithelial cells. Mol. Cell. Biol. *27*, 2155–2165.

Missero, C., Pirro, M.T., and Di Lauro, R. (2000). Multiple Ras downstream pathways mediate functional repression of the homeobox gene product TTF-1. Mol. Cell. Biol. *20*, 2783–2793.

Nagel, S., Kaufmann, M., Drexler, H.G., and MacLeod, R.A. (2003). The cardiac homeobox gene NKX2-5 is deregulated by juxtaposition with BCL11B in pediatric T-ALL cell lines via a novel t(5;14)(q35.1;q32.2). Cancer Res. *63*, 5329–5334.

Ngan, E.S., Lang, B.H., Liu, T., Shum, C.K., So, M.T., Lau, D.K., Leon, T.Y., Cherny, S.S., Tsai, S.Y., Lo, C.Y., et al. (2009). A germline mutation (A339V) in thyroid transcription factor-1 (TITF-1/NKX2.1) in patients with multinodular goiter and papillary thyroid carcinoma. J. Natl. Cancer Inst. *101*, 162–175.

Niimi, T., Nagashima, K., Ward, J.M., Minoo, P., Zimonjic, D.B., Popescu, N.C., and Kimura, S. (2001). claudin-18, a novel downstream target gene for the T/EBP/NKX2.1 homeodomain transcription factor, encodes lung- and stomach-specific isoforms through alternative splicing. Mol. Cell. Biol. *21*, 7380–7390.

Nishikawa, E., Osada, H., Okazaki, Y., Arima, C., Tomida, S., Tatematsu, Y., Taguchi, A., Shimada, Y., Yanagisawa, K., Yatabe, Y., et al. (2011). miR-375 is activated by ASH1 and inhibits YAP1 in a lineage-dependent manner in lung cancer. Cancer Res. *71*, 6165–6173.

Osada, H., Tatematsu, Y., Yatabe, Y., Horio, Y., and Takahashi, T. (2005). ASH1 gene is a specific therapeutic target for lung cancers with neuroendocrine features. Cancer Res. *65*, 10680–10685.

Osada, H., Tomida, S., Yatabe, Y., Tatematsu, Y., Takeuchi, T., Murakami, H., Kondo, Y., Sekido, Y., and Takahashi, T. (2008). Roles of achaete-scute homologue 1 in DKK1 and E-cadherin repression and neuroendocrine differentiation in lung cancer. Cancer Res. *68*, 1647–1655.

Park, K.S., Whitsett, J.A., Di Palma, T., Hong, J.H., Yaffe, M.B., and Zannini, M. (2004). TAZ interacts with TTF-1 and regulates expression of surfactant protein-C. J. Biol. Chem. *279*, 17384–17390.

Qi, J., Rice, S.J., Salzberg, A.C., Runkle, E.A., Liao, J., Zander, D.S., and Mu, D. (2012). MiR-365 regulates lung cancer and developmental gene thyroid transcription factor 1. Cell Cycle *11*, 177–186.

Ramirez, M.I., Rishi, A.K., Cao, Y.X., and Williams, M.C. (1997). TGT3, thyroid transcription factor I, and Sp1 elements regulate transcriptional activity of the 1.3-kilobase pair promoter of T1α, a lung alveolar type I cell gene. J. Biol. Chem. *272*, 26285–26294.

Runkle, E.A., Rice, S.J., Qi, J., Masser, D., Antonetti, D.A., Winslow, M.M., and Mu, D. (2012). Occludin is a direct target of thyroid transcription factor-1 (TTF-1/NKX2-1). J. Biol. Chem. *287*, 28790–28801.

Saito, R.A., Watabe, T., Horiguchi, K., Kohyama, T., Saitoh, M., Nagase, T., and Miyazono, K. (2009). Thyroid transcription factor-1 inhibits transforming growth factor-β-mediated epithelial-to-mesenchymal transition in lung adenocarcinoma cells. Cancer Res. *69*, 2783–2791.

Snyder, E.L., Watanabe, H., Magendantz, M., Hoersch, S., Chen, T.A., Wang, D.G., Crowley, D., Whittaker, C.A., Meyerson, M., Kimura, S., and Jacks, T. (2013). Nkx2-1 represses a latent gastric differentiation program in lung adenocarcinoma. Mol. Cell. Published online March 19, 2013. http://dx.doi.org/10.1016/j.molcel.2013.02.018.

Stahlman, M.T., Gray, M.E., and Whitsett, J.A. (1996). Expression of thyroid transcription factor-1 (TTF-1) in fetal and neonatal human lung. J. Histochem. Cytochem. *44*, 673–678.

Stanfel, M.N., Moses, K.A., Schwartz, R.J., and Zimmer, W.E. (2005). Regulation of organ development by the NKX-homeodomain factors: an NKX code. Cell. Mol. Biol. (Noisy-le-grand) (*Suppl 51*), OL785–OL799.

Tagne, J.B., Gupta, S., Gower, A.C., Shen, S.S., Varma, S., Lakshminarayanan, M., Cao, Y., Spira, A., Volkert, T.L., and Ramirez, M.I. (2012). Genome-wide analyses of Nkx2-1 binding to transcriptional target genes uncover novel regulatory patterns conserved in lung development and tumors. PLoS One *7*, e29907.

Takeuchi, T., Tomida, S., Yatabe, Y., Kosaka, T., Osada, H., Yanagisawa, K., Mitsudomi, T., and Takahashi, T. (2006). Expression profile-defined classification of lung adenocarcinoma shows close relationship with underlying major

genetic changes and clinicopathologic behaviors. J. Clin. Oncol. *24*, 1679–1688.

Tanaka, H., Yanagisawa, K., Shinjo, K., Taguchi, A., Maeno, K., Tomida, S., Shimada, Y., Osada, H., Kosaka, T., Matsubara, H., et al. (2007). Lineage-specific dependency of lung adenocarcinomas on the lung development regulator TTF-1. Cancer Res. *67*, 6007–6011.

Watanabe, H., Francis, J.M., Woo, M.S., Etemad, B., Lin, W., Fries, D.F., Peng, S., Snyder, E.L., Tata, P.R., Izzo, F., et al. (2013). Integrated cistromic and expression analysis of amplified NKX2-1 in lung adenocarcinoma identifies LMO3 as a functional transcriptional target. Genes Dev. *27*, 197–210.

Weir, B.A., Woo, M.S., Getz, G., Perner, S., Ding, L., Beroukhim, R., Lin, W.M., Province, M.A., Kraja, A., Johnson, L.A., et al. (2007). Characterizing the cancer genome in lung adenocarcinoma. Nature *450*, 893–898.

Wert, S.E., Dey, C.R., Blair, P.A., Kimura, S., and Whitsett, J.A. (2002). Increased expression of thyroid transcription factor-1 (TTF-1) in respiratory epithelial cells inhibits alveolarization and causes pulmonary inflammation. Dev. Biol. *242*, 75–87.

Winslow, M.M., Dayton, T.L., Verhaak, R.G., Kim-Kiselak, C., Snyder, E.L., Feldser, D.M., Hubbard, D.D., DuPage, M.J., Whittaker, C.A., Hoersch, S., et al. (2011). Suppression of lung adenocarcinoma progression by Nkx2-1. Nature *473*, 101–104.

Yamaguchi, T., Yanagisawa, K., Sugiyama, R., Hosono, Y., Shimada, Y., Arima, C., Kato, S., Tomida, S., Suzuki, M., Osada, H., and Takahashi, T. (2012). NKX2-1/TITF1/TTF-1-induced ROR1 is required to sustain EGFR survival signaling in lung adenocarcinoma. Cancer Cell *21*, 348–361.

Yan, C., and Whitsett, J.A. (1997). Protein kinase A activation of the surfactant protein B gene is mediated by phosphorylation of thyroid transcription factor 1. J. Biol. Chem. *272*, 17327–17332.

Yan, C., Naltner, A., Conkright, J., and Ghaffari, M. (2001). Protein-protein interaction of retinoic acid receptor α and thyroid transcription factor-1 in respiratory epithelial cells. J. Biol. Chem. *276*, 21686–21691.

Yan, C., Naltner, A., Martin, M., Naltner, M., Fangman, J.M., and Gurel, O. (2002). Transcriptional stimulation of the surfactant protein B gene by STAT3 in respiratory epithelial cells. J. Biol. Chem. *277*, 10967–10972.

Yang, L., Yan, D., Bruggeman, M., Du, H., and Yan, C. (2004). Mutation of a lysine residue in a homeodomain generates dominant negative thyroid transcription factor 1. Biochemistry *43*, 12489–12497.

Yatabe, Y., Mitsudomi, T., and Takahashi, T. (2002). TTF-1 expression in pulmonary adenocarcinomas. Am. J. Surg. Pathol. *26*, 767–773.

Yatabe, Y., Kosaka, T., Takahashi, T., and Mitsudomi, T. (2005). EGFR mutation is specific for terminal respiratory unit type adenocarcinoma. Am. J. Surg. Pathol. *29*, 633–639.

Yin, Z., Gonzales, L., Kolla, V., Rath, N., Zhang, Y., Lu, M.M., Kimura, S., Ballard, P.L., Beers, M.F., Epstein, J.A., and Morrisey, E.E. (2006). Hop functions downstream of Nkx2.1 and GATA6 to mediate HDAC-dependent negative regulation of pulmonary gene expression. Am. J. Physiol. Lung Cell. Mol. Physiol. *291*, L191–L199.

Yuan, B., Li, C., Kimura, S., Engelhardt, R.T., Smith, B.R., and Minoo, P. (2000). Inhibition of distal lung morphogenesis in Nkx2.1(−/−) embryos. Dev. Dyn. *217*, 180–190.

Zhou, B., Zhong, Q., Minoo, P., Li, C., Ann, D.K., Frenkel, B., Morrisey, E.E., Crandall, E.D., and Borok, Z. (2008). Foxp2 inhibits Nkx2.1-mediated transcription of SP-C via interactions with the Nkx2.1 homeodomain. Am. J. Respir. Cell Mol. Biol. *38*, 750–758.

Oncogene (2013) **32,** 3559–3568

www.nature.com/onc

ONCOGENOMICS

The DNA methylation landscape of small cell lung cancer suggests a differentiation defect of neuroendocrine cells

S Kalari[1,4], M Jung[1,4], KH Kernstine[2,5], T Takahashi[3] and GP Pfeifer[1]

Small cell lung cancer (SCLC) is a disease characterized by aggressive clinical behavior and lack of effective therapy. Owing to its tendency for early dissemination, only a third of patients have limited-stage disease at the time of diagnosis. SCLC is thought to derive from pulmonary neuroendocrine cells. Although several molecular abnormalities in SCLC have been described, there are relatively few studies on epigenetic alterations in this type of tumor. Here, we have used methylation profiling with the methylated-CpG island recovery assay in combination with microarrays and conducted the first genome-scale analysis of methylation changes that occur in primary SCLC and SCLC cell lines. Among the hundreds of tumor-specifically methylated genes discovered, we identified 73 gene targets that are methylated in >77% of primary SCLC tumors, most of which have never been linked to aberrant methylation in tumors. These methylated targets have potential for biomarker development for early detection and therapeutic management of SCLC. SCLC cell lines had a greater number of hypermethylated genes than primary tumors. Gene ontology analysis indicated a significant enrichment of methylated genes functioning as transcription factors and in processes of neuronal differentiation. Motif analysis of tumor-specific methylated regions identified enrichment of binding sites for several neural cell fate-specifying transcription factors including NEUROD1, HAND1, ZNF423 and REST. We hypothesize that two potential mechanisms, loss of cell fate-determining transcription factors by methylation of their promoters and functional inactivation of their corresponding genomic-binding sites by DNA methylation, can promote a differentiation defect of neuroendocrine cells thus enhancing the ability of tumor progenitor cells to transition toward SCLC.

Oncogene (2013) **32,** 3559–3568; doi:10.1038/onc.2012.362; published online 20 August 2012

Keywords: DNA methylation; small cell lung cancer; differentiation; epigenetics

INTRODUCTION

Lung cancer is divided by histology into small cell lung cancer (SCLC) and non-small cell lung cancer (NSCLC). SCLC represents about 15% of all lung cancer cases and is one of the most lethal forms of cancer with properties of high mitotic rate and early metastasis.[1] It is distinctly characterized by small cells with poorly defined cell borders and minimal cytoplasm, rare nucleoli and finely granular chromatin. Although SCLC patients initially respond to chemotherapy and radiation therapy, the disease recurs in the majority of patients. Because of the aggressiveness of SCLC and the lack of effective therapy and early diagnosis, without treatment the median survival time for SCLC is only 2–4 months. With current treatment modalities, the median survival times for limited-stage disease, <5% of the total, is 16–24 months and for extensive disease, 7–12 months, in spite of the fact that 60–80% of patients respond to therapy. It is essential to gain a better understanding of the molecular pathogenesis of the disease and to identify molecular alterations, which could lead to improved results in early detection and a means of assessing response to therapy.

Several studies have identified abnormalities within tumor suppressor genes, oncogenes, signaling pathways, receptor kinases and growth factors that have a proven role in the pathogenesis of various other human cancers. About 90% of SCLC patients' DNA samples have mutations in the *TP53* gene.[2,3] Similarly, another tumor suppressor gene, retinoblastoma, is either deleted or mutated in the majority (about 90%) of SCLCs.[2,4] In addition, higher expression of the *MYC* family of oncogenes has been found in SCLC cell lines, xenografts and fresh tumor specimens.[5–7] Abnormalities in various receptor tyrosine kinase families are commonly found in the majority of SCLC cases. These changes are associated with a more aggressive tumor growth, resistance to therapy and poor prognosis.[8,9] The phosphoinositide 3-kinase/AKT pathway is defective in SCLC patients' tumors. Nearly two thirds of SCLCs have phosphorylated AKT[9] and this constitutively active kinase can modulate a variety of cellular functions such as cell proliferation, survival, motility, adhesion and differentiation.[8] The cellular origin of SCLC is yet to be proven definitively. Recent studies in mice indicated that neuroendocrine cells seem to be the predominant cells of origin of SCLC.[10,11]

SCLC is also characterized by common deletion of the *fragile histidine triad (FHIT)* gene, located at 3p14.[2] Similarly, chromosome 3p21 is another locus, which is frequently subjected to loss in almost all SCLCs, and this event is thought to be an early event in lung cancer pathogenesis.[12] At 3p21.3, there are several candidate tumor suppresser genes, including the Ras association domain family member 1A (*RASSF1A*), tumor suppressor candidate 2

[1]Department of Cancer Biology, Beckman Research Institute of the City of Hope, Duarte, CA, USA; [2]Department Surgery, Beckman Research Institute of the City of Hope, Duarte, CA, USA and [3]Division of Molecular Carcinogenesis, Nagoya University Graduate School of Medicine, Nagoya, Japan. Correspondence: Dr GP Pfeifer, Department of Cancer Biology, Beckman Research Institute, City of Hope, Duarte, CA 91010, USA.
E-mail: gpfeifer@coh.org
[4]These authors contributed equally to this work.
[5]Current address: Division of Thoracic Surgery, University of Texas Southwestern Medical Center, Dallas, TX, USA.
Received 10 September 2011; revised 18 May 2012; accepted 4 July 2012; published online 20 August 2012

(*TUSC2*, also known as *FUS1*), semaphorin 3B (*SEMA3B*) and semaphorin 3F (*SEMA3F*).[13,14]

In contrast to the genetic alterations discussed above, epigenetic aberrations, specifically DNA methylation changes found in SCLC tumors, have not been studied so far in a comprehensive manner. DNA methylation analysis might provide vital information that could shed light on mechanisms of disease initiation, development and progression, as well as lead to cancer biomarker discovery.[15,16] There are several gene-specific DNA methylation studies for SCLC. For example, promoter hypermethylation of the tumor suppressor gene *RASSF1A* and subsequent suppression of its expression is found in almost all of the SCLC tumors.[17,18] Another study found *caveolin-1* (*CAV1*) gene methylation in over 90% the tested SCLC cell lines.[19]

Lack of genome-wide DNA methylation studies in SCLC prompted us to undertake this task. We applied the methylated-CpG island recovery assay (MIRA), which has shown excellent sensitivity for identification of methylated genomic regions in cancer,[20–23] to map DNA methylation patterns at promoters and CpG islands of primary SCLC tumors, SCLC cell lines and normal lung control samples.

RESULTS

Identification of methylated genes in human SCLC tissue on a genome-wide platform

The MIRA technique, used in combination with microarray analysis, is a high-resolution mapping technique and has proven successful for profiling global DNA methylation patterns in NSCLC and other tumors.[22–25] In this study, we have applied this sensitive method to study the methylation status of CpG islands and promoters in SCLC to investigate the potential role of methylation changes in the initiation and development of SCLC, as well as to discover potential biomarkers for better management of the disease. Eighteen human primary SCLC and five SCLC cell line DNA samples were screened for methylation by MIRA-based microarrays. DNAs from five normal healthy lung tissues adjacent to the tumor and obtained at the time of surgical resection were used as controls in the MIRA analysis. DNA was subjected to MIRA enrichment as described previously[26,27] and subsequent microarray analysis was performed on 720k Nimblegen CpG island plus promoter arrays.

Microarray data analysis

To increase the specificity of MIRA-based enrichment signals, we chose to call peaks based on different quantiles of four neighboring probes. Peaks were then calculated using the base functions of the Bioconductor package Ringo.[28] Table 1 shows the specificity and sensitivity of this approach relative to different quantile ranges using DNA from the SCLC cell line SW1271. Based on the validations conducted by combined bisulfite restriction analysis (COBRA) single-gene methylation assays, we chose an 80% cutoff for medium to strongly methylated regions and a cutoff below 56% defined as not methylated. Thus, compared with the conventional NimbleScan method using the default settings, we could increase the sensitivity of methylation peak detection to 94% without decreasing specificity. As this threshold was defined for one SCLC cell line, we tested the same settings for primary small lung cancer samples and did not observe a significant increase of false positive predicted hypermethylated regions.

Using the peak identification algorithm described in the Materials and methods section, we identified ~15 000 methylation peaks in each sample (Supplementary Table 1). Our clustering analysis of tumor samples and controls showed that SCLC cell lines clustered together and that four of the five normal samples were close to each other, but different tumor samples occupied different spaces in the dendrogram (Supplementary Figure 1).

Table 1. Validation of microarray results by COBRA assays

Top quantile (%)	*No. of targets tested*[a]	*Met*	*UnMet*	*PCR fails*	*% Met*	*% UnMet*
99	10	9	—	1	100	0
95	10	9	—	1	100	0
90	10	9	1	—	90	10
85	10	9	1	—	90	10
80	10	7	3	—	70	30
70	14	3	5	6	37.5	62.5
60	19	3	12	4	20	80
50	13	2	11	—	15	85

Abbreviations: COBRA, combined bisulfite restriction analysis; Met, methylated; UnMet, unmethylated. [a]COBRA was performed for each quantile category with bisulfite-converted DNA from the SW1271 cell line. Results were tabulated for number of Met and UnMet genes in these various categories.

Taking into account that we had 18 tumor samples and 5 normal samples for microarray data analysis, we defined a stringent tumor-specific methylated region as the overlapping region that meets the minimum 80% quantile criterion in 14 of 18 tumors and is below the 56% quantile in 4 of 5 normal tissues. A less stringent set was defined as an overlap between at least 6 peaks from tumor samples out of 18, using the same criteria as above. Thus, we were mainly comparing strongly methylated regions versus poorly methylated regions. Although small methylation level differences could not be picked up this way, the aim of discovering uniquely strongly methylated and tumor-specific regions was well supported by this approach.

Methylated genes in primary SCLC

Supplementary Figure 2 shows examples of tumor-specific methylation peaks at the *PROX1, CCDC140, PAX3 and SIM1* genes located on chromosomes 1, 2 and 6, respectively. Supplementary Figure 3 shows extensive tumor-specific methylation of the *HOXD* cluster on chromosome 2. Compilation of tumor-specific methylation peaks revealed a total of 698 regions in 6 out of 18 tumors (≥33% of SCLC tumors) compared with normal lung DNA, which represented 339 ensembl gene IDs for promoter-related tumor-specifically methylated regions (defined as −5000 to +1000 relative to the TSS), 197 ensembl gene IDs related to peaks mapped to the gene bodies and 63 ensembl gene IDs for peaks mapped downstream of the corresponding genes (Figure 1a; Supplementary Table 2). Individual primary SCLCs contained between 366 and almost 1500 tumor-specific methylation peaks (Supplementary Table 3).

There were 73 tumor-specific methylated peaks, which were found in at least 14 out of 18 SCLC tumors (>77% of SCLC tumors), that corresponded to 28 ensembl gene IDs for promoters, 30 ensembl gene IDs for gene bodies and 11 for downstream regions (Figure 1b). These methylated genes from 77% or more of the SCLC tumors are presented in Table 2 and in Supplementary Table 4, for more detailed information.

Identification of methylated genes in human SCLC lines

Owing to the limited availability of primary SCLC tissue, we added several SCLC cell lines originally derived from primary tumor sites. Owing to the unavailability of neuroendocrine cells, which are believed to be the cell of origin of SCLC,[10] we chose normal bronchial epithelial cells as a control for these studies. Clustering analysis based on the total methylation peaks of SCLC cell lines showed that all cell lines cluster tightly together (Supplementary Figure 1). Further analysis of these methylated peaks for tumor cell line-specific peaks revealed 1223 unique tumor-specific peaks found in 4 out of 5 SCLC cell lines (≥80% of SCLC cell lines)

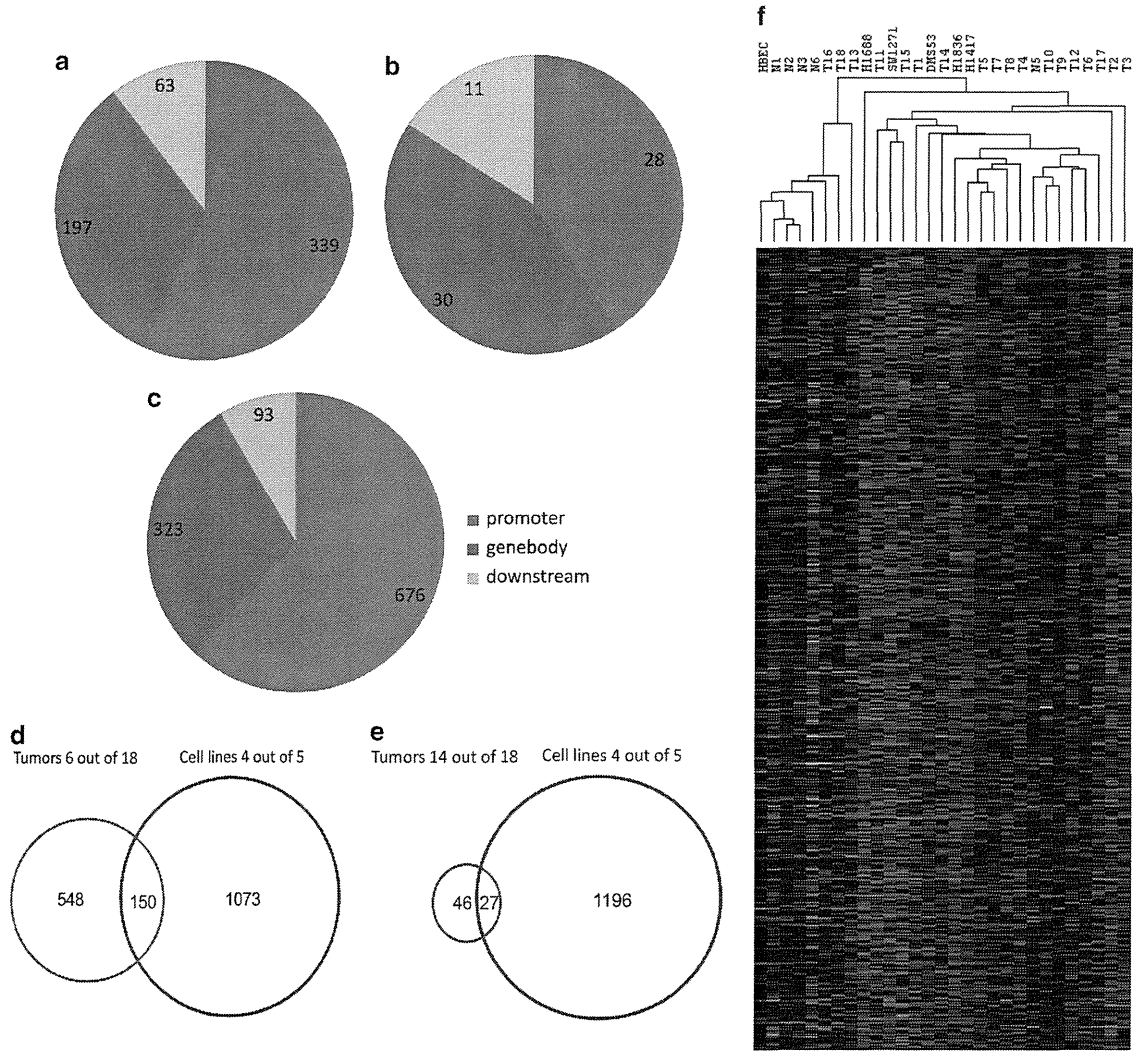

Figure 1. Mapping of tumor-specific methylation peaks in primary SCLC and SCLC cell lines. (**a**) Localization of the methylation peaks in primary SCLC (6 or more out of 18 tumors methylated; that is, peaks that meet the minimum 80% quantile criterion in 6 of 18 tumors) relative to gene position. (**b**) Localization of the methylation peaks in primary SCLC (14 or more out of 18 tumors methylated) relative to gene position. (**c**) Localization of the methylation peaks in SCLC cell lines (4 or more out of 5 cell lines methylated) relative to gene position. (**d**) Overlap of methylation peaks between SCLC primary tumors (6 or more out of 18 tumors methylated) and SCLC cell lines (4 or more out of 5 cell lines methylated). (**e**) Overlap of methylation peaks between SCLC primary tumors (14 or more out of 18 tumors methylated) and SCLC cell lines (4 or more out of 5 cell lines methylated). (**f**) Cluster analysis of methylation peaks. Methylation peaks found in at least 33% of tumor samples but not in normal samples were identified. Then the data were subjected to hierarchical clustering with Euclidean distance and average linkage method using Cluster v3.0 (http://bonsai.hgc.jp/~mdehoon/software/cluster/software.htm) and visualized in Java TreeView (http://jtreeview.sourceforge.net). Red, methylated state; green, unmethylated state.

compared with methylated peaks form normal bronchial epithelial cells (Supplementary Table 5). These peaks represented 676 ensembl gene IDs mapped to promoter regions, 323 ensembl gene IDs corresponding to methylated regions in the gene body and 93 ensembl gene IDs where the hypermethylated regions could be located downstream of genes (Figure 1c). Individual cell lines contained between 2779 and 4485 cell line-specific methylation peaks (Supplementary Table 3), numbers that were greater than those found in primary SCLCs. We compared SCLC tumor-specific methylated regions with SCLC cell line-specific methylated regions. There was a relatively small group ($<20\%$) of SCLC cell line-specific genes found to be commonly (>6 of 18) methylated in primary SCLC tumors and vice versa (that is, $\sim 21\%$ of SCLC primary tumor peaks matched with those of frequent SCLC cell line methylation; Figure 1d). When we determined the overlap between peaks methylated in 14/18 tumors and 4 of 5 cell lines, the number of overlapped genes was 27 (Figure 1e). We mapped the location of tumor-specific methylation peaks relative to promoters, gene bodies and locations downstream of genes (Figures 1a–c). The distribution patterns were similar for peaks found in $\geqslant 6/18$ tumors and in cell lines, but for the most frequently methylated genes ($\geqslant 14/18$) the peaks tended to be more commonly localized in gene bodies and downstream (Figure 1b). Cluster analysis of methylation peaks in normal and tumor samples is shown in Figure 1f.

Validation of gene-specific methylation in SCLC samples

We further validated tumor-specific methylation peaks discovered by microarray analysis for several of the targets by the COBRA assay. In this assay, bisulfite-converted DNA is PCR-amplified using gene-specific primers and is then digested with a restriction

Table 2. Gene targets methylated in 77% or more of primary SCLCs

Chromosome	*Start peak*	*End peak*	*hgnc_symbol*	*Description*
6	27647872	27648246		
1	91189238	91189687	BARHL2	BarH-like homeobox 2 [Source:HGNC Symbol;Acc:954]
10	124901911	124902685	HMX2	H6 family homeobox 2 [Source:HGNC Symbol;Acc:5018]
15	53087134	53087683	ONECUT1	One cut homeobox 1 [Source:HGNC Symbol;Acc:8138]
9	100611180	100611554	FOXE1	Forkhead box E1 (thyroid transcription factor 2) [Source:HGNC Symbol;Acc:3806]
17	59529794	59530268	TBX4	T-box 4 [Source:HGNC Symbol;Acc:11603]
1	214153078	214153777	PROX1	Prospero homeobox 1 [Source:HGNC Symbol;Acc:9459]
14	95239173	95240547	GSC	Goosecoid homeobox [Source:HGNC Symbol;Acc:4612]
21	38068981	38069055	SIM2	Single-minded homolog 2 (Drosophila) [Source:HGNC Symbol;Acc:10883]
6	117584283	117584857	VGLL2	Vestigial-like 2 (Drosophila) [Source:HGNC Symbol;Acc:20232]
14	37124350	37124799	PAX9	Paired box 9 [Source:HGNC Symbol;Acc:8623]
2	177004205	177004604		
14	36991675	36992549	NKX2-1	NK2 homeobox 1 [Source:HGNC Symbol;Acc:11825]
1	197879403	197880252	LHX9	LIM homeobox 9 [Source:HGNC Symbol;Acc:14222]
11	32455050	32455624	WT1-AS	WT1 antisense RNA (non-protein coding) [Source:HGNC Symbol;Acc:18135]
13	112719925	112720174	SOX1	SRY (sex-determining region Y)-box 1 [Source:HGNC Symbol;Acc:11189]
21	38069706	38069780	SIM2	Single-minded homolog 2 (Drosophila) [Source:HGNC Symbol;Acc:10883]
2	176956605	176956754	HOXD13	Homeobox D13 [Source:HGNC Symbol;Acc:5136]
9	129566330	129566704	ZBTB43	Zinc finger and BTB domain containing 43 [Source:HGNC Symbol;Acc:17908]
3	172167182	172167256	GHSR	Growth hormone secretagogue receptor [Source:HGNC Symbol;Acc:4267]
1	230777303	230777452	COG2	Component of oligomeric golgi complex 2 [Source:HGNC Symbol;Acc:6546]
3	27765097	27765996	EOMES	Eomesodermin [Source:HGNC Symbol;Acc:3372]
20	30639265	30639939	HCK	Hemopoietic cell kinase [Source:HGNC Symbol;Acc:4840]
3	183274057	183274331	KLHL6	Kelch-like 6 (Drosophila) [Source:HGNC Symbol;Acc:18653]
12	114846668	114847217	TBX5	T-box 5 [Source:HGNC Symbol;Acc:11604]
4	122685401	122685475		Uncharacterized protein [Source:UniProtKB/TrEMBL;Acc:E7ENT1]
2	182547581	182547655		
20	44880344	44880693	CDH22	Cadherin 22, type 2 [Source:HGNC Symbol;Acc:13251]
9	21402751	21403100	IFNA12P	Interferon, alpha 12, pseudogene [Source:HGNC Symbol;Acc:5443]
7	97360940	97362189	TAC1	Tachykinin, precursor 1 [Source:HGNC Symbol;Acc:11517]
2	223162732	223163206	CCDC140	Coiled-coil domain containing 140 [Source:HGNC Symbol;Acc:26514]
7	129422815	129423514		
2	192711381	192711755		
6	27107272	27107346	HIST1H4I	Histone cluster 1, H4i [Source:HGNC Symbol;Acc:4793]
2	176969205	176970504	HOXD11	Homeobox D11 [Source:HGNC Symbol;Acc:5134]
19	9608951	9609250	ZNF560	Zinc finger protein 560 [Source:HGNC Symbol;Acc:26484]
7	27282651	27282900	EVX1	Even-skipped homeobox 1 [Source:HGNC Symbol;Acc:3506]
2	223163332	223163406	PAX3	Paired box 3 [Source:HGNC Symbol;Acc:8617]
7	27282951	27283025	EVX1	Even-skipped homeobox 1 [Source:HGNC Symbol;Acc:3506]
7	8474326	8475225	NXPH1	Neurexophilin 1 [Source:HGNC Symbol;Acc:20693]
4	174452351	174452925		Nbla00301 (NBLA00301), non-coding RNA [Source:RefSeq DNA;Acc:NR_003679]
4	13545178	13545427	NKX3-2	NK3 homeobox 2 [Source:HGNC Symbol;Acc:951]
X	111325120	111325194	TRPC5	Transient receptor potential cation channel, subfamily C, member 5 [Source:HGNC Symbol;Acc:12337]
6	100911555	100911904	SIM1	Single-minded homolog 1 (Drosophila) [Source:HGNC Symbol;Acc:10882]
14	29243250	29243899	C14orf23	Chromosome 14 open-reading frame 23 [Source:HGNC Symbol;Acc:19828]
5	172660770	172660844	NKX2-5	NK2 transcription factor related, locus 5 (Drosophila) [Source:HGNC Symbol;Acc:2488]
2	220196257	220197006	RESP18	Regulated endocrine-specific protein 18 homolog (rat) [Source:HGNC Symbol;Acc:33762]
9	126776030	126776479	LHX2	LIM homeobox 2 [Source:HGNC Symbol;Acc:6594]
1	165323302	165323951	LMX1A	LIM homeobox transcription factor 1, alpha [Source:HGNC Symbol;Acc:6653]
2	119603031	119603180	EN1	Engrailed homeobox 1 [Source:HGNC Symbol;Acc:3342]
12	63543634	63544008	AVPR1A	Arginine vasopressin receptor 1A [Source:HGNC Symbol;Acc:895]
8	97170050	97170499	GDF6	Growth differentiation factor 6 [Source:HGNC Symbol;Acc:4221]
1	47694839	47695213	TAL1	T-cell acute lymphocytic leukemia 1 [Source:HGNC Symbol;Acc:11556]
13	84453425	84453824	SLITRK1	SLIT and NTRK-like family, member 1 [Source:HGNC Symbol;Acc:20297]
4	174448251	174448725	HAND2	Heart and neural crest derivatives expressed 2 [Source:HGNC Symbol;Acc:4808]
2	176977280	176977729	HOXD10	Homeobox D10 [Source:HGNC Symbol;Acc:5133]
5	37835994	37836168	GDNF	Glial cell-derived neurotrophic factor [Source:HGNC Symbol;Acc:4232]
9	37029751	37030525	PAX5	Paired box 5 [Source:HGNC Symbol;Acc:8619]
14	29247325	29247499	C14orf23	Chromosome 14 open reading frame 23 [Source:HGNC Symbol;Acc:19828]
7	8483051	8483825	NXPH1	Neurexophilin 1 [Source:HGNC Symbol;Acc:20693]
6	154360508	154360857	OPRM1	Opioid receptor, mu 1 [Source:HGNC Symbol;Acc:8156]
20	58569381	58569455	CDH26	Cadherin 26 [Source:HGNC Symbol;Acc:15902]
9	21968201	21968875	C9orf53	Chromosome 9 open reading frame 53 [Source:HGNC Symbol;Acc:23831]
16	49311725	49312274	CBLN1	Cerebellin 1 precursor [Source:HGNC Symbol;Acc:1543]
8	9756191	9756540	MIR124-1	MicroRNA 124-1 [Source:HGNC Symbol;Acc:31502]
5	170741921	170741995	TLX3	T-cell leukemia homeobox 3 [Source:HGNC Symbol;Acc:1353]
20	21488326	21488925	NKX2-2	NK2 homeobox 2 [Source:HGNC Symbol;Acc:7835]
5	170743496	170744170	TLX3	T-cell leukemia homeobox 3 [Source:HGNC Symbol;Acc:13532]